October 1990

CfPA-TH-90-001
BA-90-79

UNIVERSITY OF CALIFORNIA, BERKELEY

CENTER FOR PARTICLE ASTROPHYSICS

Three Exceptions in the Calculation of Relic Abundances

KIM GRIEST

Center for Particle Astrophysics and Astronomy Department, University of California, Berkeley, CA 94720

and

DAVID SECKEL

Bartol Research Institute, University of Delaware, Newark, DE 19716

ABSTRACT

Calculation of relic abundances of elementary particles by following their annihilation and freeze-out in the early universe has become an important and standard tool in discussing particle dark matter candidates. We find three situations, all occurring in the literature, in which the standard methods of calculating relic abundances fail. The first situation occurs when another particle lies near in mass to the relic particle and shares a quantum number with it. An example is a light squark with neutralino dark matter. The additional particle must be included in the reaction network, since its annihilation can control the relic abundance. The second situation occurs when the relic particle lies near a mass threshold. Previously, annihilation into particles heavier than the relic particle was considered kinematically forbidden, but we show that if the mass difference is $\sim 5\% - 15\%$, these "forbidden" channels can dominate the cross section and determine the relic abundance. The third situation occurs when the annihilation takes place near a pole in the cross section. Proper treatment of the thermal averaging and the annihilation after freeze-out shows that the dip in relic abundance caused by a pole is not nearly as sharp or deep as previously thought.

Introduction

The calculation of the present day density of elementary particles which were in thermal equilibrium in the early Universe has become quite commonplace.[1] Of particular interest is the so called Lee-Weinberg[2,3] calculation in which annihilation after a particle species has become non-relativistic determines the present day abundance of that species. Standard approximate solutions to the Boltzmann equation exist for this calculation and have been tested numerically. In this paper we wish to point out three cases where naive application of the standard methods fail to give correct results and a modified treatment is required. All three cases exist in the literature and in all three cases erroneous conclusions have been drawn. For each case, we present appropriate approximate solutions to the Boltzmann equation(s) and describe the values of the parameters for which they apply.

The first case occurs when the relic particle is the lightest of a set of similar particles whose masses are nearly degenerate. In this case the relic abundance of the lightest particle is determined not only by its annihilation cross section, but also by the annihilation of the heavier particles, which will later decay into the lightest. We call this the case of "co-annihilation". As an example, consider a supersymmetric theory in which the scalar quarks or scalar electrons are only slightly more massive than the lightest supersymmetric particle (LSP), usually taken to be a neutralino. Previous calculations of the relic abundance which consider only the LSP annihilation can be in error by more than two orders of magnitude.

The second case concerns annihilation into particles which are more massive than the relic particle. Previous treatments regarded this as kinematically forbidden, but we show that if the heavier particles are only 5-15% more massive, these channels can dominate the annihilation cross section and determine the relic abundance. We call this the "forbidden" channel annihilation case. Examples include annihilation into $b\bar{b}$, $t\bar{t}$, W^+W^-, or Higgs bosons, when the annihilating particle is lighter than the the final state particle.

The third case occurs when the annihilation takes place near a pole in the cross section. This happens, for example, in Z^0 exchange annihilation when the mass of the relic particle is near $m_Z/2$. Previous treatments have incorrectly handled the thermal averages and the integration of the Boltzmann equation in these situations. The dip

in relic abundance caused by a pole is broader and not nearly as deep as previous treatments imply.[4]

For all three cases we present simple formulas which allow for a more correct treatment. We also present examples for each case and describe the precise conditions under which the modified treatment is necessary. In Section II we review the standard method for performing the 'Lee-Weinberg' calculation, and describe the approximations within which we will work. In Section III we discuss the "co-annihilation" case, in Section IV we discuss the "forbidden" channel case; and in Section V we discuss annihilation near a pole.

II. Standard Calculation of Relic Abundance

Here, we summarize the standard technique for calculating the relic abundance of a particle species, χ, in the Lee-Weinberg scenario. First a note about the philosophy of this presentation. We are considering cases where the 'standard' technique fails by a factor of two or more, and so we wish to highlight the modifications necessary to avoid these gross errors. Thus, we are not overly concerned with $10-20\%$ corrections, and our presentation will not emphasize some recent improvements[3] which make the calculations more precise, but more cumbersome.

The relic abundance is found by solving the Boltzmann equation for the evolution of the χ number density, n,

$$\frac{dn}{dt} = -3Hn - \langle\sigma v\rangle\,(n^2 - (n^{eq})^2), \tag{1}$$

where H is the Hubble parameter, n^{eq} is the χ equilibrium number density, v is the "relative velocity", and $\langle\sigma v\rangle$ is the thermal average of the annihilation cross section ($\chi + \chi \to$ all). For the equilibrium number density we will use the non-relativistic approximation $n^{eq} \approx g(mT/2\pi)^{3/2}\exp(-m/T)$, where g is the number of spin, color, etc. degrees of freedom of χ, T is the temperature and m is the mass of the relic. For particles which may potentially play the role of cold dark matter, the relevant temperatures are of order $m/25$ and the non-relativistic equilibrium abundance is well justified. Typically[5] the cross section is Taylor expanded in v^2 before the thermal average is taken, $\sigma = a + bv^2$. The thermal average then shows a linear temperature dependence $\langle\sigma v\rangle = a + 6bT/m$.

Eq. (1) can be solved numerically, but a convenient and accurate approximation exists. At early times n is approximated by n^{eq}, but as the temperature drops below the mass m, n^{eq} drops exponentially and eventually a point, denoted "freeze-out",

is reached where the reaction rate is not fast enough to maintain equilibrium. From this point on, the n^{eq} term in Eq. (1) can be ignored and the resulting equation is easily integrated. Thus, the solution of Eq. (1) is given by solving in two regimes and matching those solutions at the 'freezeout' point.

For ease of presentation we will follow the method detailed in Ref. 1. The freezeout point is given in terms of the scaled inverse temperature $x = m/T$,

$$x_f = \ln \frac{.038 g m_{pl} m \langle \sigma v \rangle}{{g_*}^{1/2} x_f^{1/2}}, \tag{2}$$

where $m_{pl} = 1.22 \times 10^{19}$ GeV, and g_* is the total number of effectively relativistic degrees of freedom at the time of freezeout. Eq. (2) is usually solved iteratively. In Ref. 1 this is done analytically by substituting for x_f on the right side of Eq. (2). For the cases considered in this paper the thermal averaged cross-section changes rapidly with temperature and we will take a numerical approach to solving Eq. (2).

At freezeout the abundance of relic particles is usually taken to be the equilibrium abundance; however, after freezeout there is further significant annihilation of relic particles which reduces the abundance to its final and present value. The efficiency of this post-freeze out annihilation is expressed through the integral J,

$$J(x_f) = \int_{x_f}^{\infty} \frac{\langle \sigma v \rangle}{x^2} dx. \tag{3}$$

The present day mass density of χ particles is then given by

$$\Omega h^2 \approx \frac{1.07 \times 10^9 \text{ GeV}^{-1}}{J {g_*}^{1/2} m_{pl}}, \tag{4}$$

where Ω is the present day mass density divided by the critical density for closure and h is the present day Hubble parameter[6] in units of 100 km s^{-1} Mpc^{-1}. For the standard scenarios where $\langle \sigma v \rangle$ is expressed in terms of its Taylor expansion the present day abundance of χ particles is approximately

$$\Omega h^2 = \frac{1.07 \times 10^9 x_f}{{g_*}^{1/2} m_{pl}(\text{GeV})(a + 3b/x_f)}, \tag{5}$$

We now list the known weaknesses with the calculation as summarized above. First, as already mentioned, the derivation assumes the non-relativistic approximation

in calculating equilibrium abundances. It also assumes a non-relativistic approach in calculating thermal average cross-sections, and as pointed out in Ref. 3 this may lead to 10% errors. Next, the derivation assumes that g_* remains constant throughout the period of annihilation, which is not generally correct. The approximation is worst when freezeout occurs during the quark-hadron transition, but even in this case the errors[3,7] are not large. Except where noted, we will ignore these small omissions for the remainder of this paper.

Potentially more problematic, for our discussion, is the determination of x_f, or the matching point for the two regimes where the Boltzmann equation may be easily solved. The value of x_f is derived by assuming that at early times $n \approx n^{eq}$. It is then simple to solve for the difference $\delta = n - n^{eq}$. The freeze out point is given by when $\delta = cn^{eq}$, where the constant c is determined empirically by comparing to some numerical integrations of the Boltzmann equation. For annihilation cross-sections that are relatively temperature insensitive, the choice of c is not critical. A convenient choice[8] for thermal averaged cross-sections with power law temperature dependence, $\langle\sigma v\rangle \sim T^n$, is $c(c+2) = n+1$. The value of x_f given in Eq. (2) uses $n = 0$, $c = \sqrt{2}-1$.

For the cases discussed later in this paper the question of matching and determination of x_f may have to be readdressed since the cross-sections we consider have much stronger temperature dependences than simple power laws. Thus, whereas a small error in x_f usually makes little difference to the annihilation integral J, in our case it may. With this in mind, for most of our paper we present results based on the use of Eq. (2) ($c = \sqrt{2} - 1$); however, we will show some explicit numerical integrations of the Boltzmann equation to show that this choice does not lead to large errors.

The plan for the remainder of this paper is now straightforward. a) Put the problem in the form of Eq. (1). b) Solve for x_f using Eq. (2) and an appropriate $\langle\sigma v\rangle$. c) Evaluate the annihilation integral, J, and plug the result into Eq. (4). The vital point in the above procedure is to use an appropriate $\langle\sigma v\rangle$ in steps b) and c).

III. Relic Abundance from Co-annihilation

The first two cases we discuss, "co-annihilation" and the case of the "forbidden channel", have a common theme. In both cases particles are presumed to exist which are nearly degenerate with, but have masses slightly greater than, the relic, here denoted by χ_1. If the mass difference, $\delta m \equiv m - m_1$, is large compared to the temperature T_f, when χ_1 annihilations freezeout, then the extra particles play no significant role. However, if $\delta m \approx T_f$ the extra particles are thermally accessible. In the co-annihilation case, this implies that the extra particles will be nearly as abundant

as the relic species. Given that T_f is of order $m_1/25$ for cases of interest, if the mass degeneracy holds at the $\sim 5-10\%$ level, annihilations involving the extra particles can play a significant role in determining the relic abundance.

Consider the evolution in the early Universe of a class of particles, χ_i, $i = 1, \cdots, N$ which differ from Standard Model particles by a multiplicatively conserved quantum number. Examples include the supersymmetric particles under R-parity and the pseudo-Higgs particles of Ref. 9 under their symmetry. We assume that the particles are labeled such that $m_i < m_j$, when $i < j$; that is χ_1 has mass m_1 and is the lightest, while χ_2 is the second lightest, etc. Note that since we are interested in the case where the lightest of these particles is stable and perhaps even a dark matter candidate, the assumption of the existence of a conserved quantum number is not particularly ad hoc. Reactions of the following types change the χ_i number densities and determine their abundances in the early universe.

$$\chi_i \chi_j \leftrightarrow X X' \tag{6a}$$

$$\chi_i X \leftrightarrow \chi_j X' \tag{6b}$$

$$\chi_j \leftrightarrow \chi_i X X' \tag{6c}$$

where X, X' denote any Standard Model particles. There may be many choices for the pair X and X', but generally they are not independent; a choice of χ_i, χ_j and X will determine X'. Reactions such as $\chi_i \chi_j \leftrightarrow \chi_k X$ and $\chi_i X \leftrightarrow X X$ are forbidden by the assumed symmetry. Note that as long as reactions of type (6c) take place at a reasonable rate, we expect all the χ_j $(j > 1)$ particles to have decayed into χ_1 particles by today. In the example of supersymmetry, χ_1 would be the LSP and χ_j $(j > 1)$ would be the squarks, etc.

The abundances of the χ_i are determined by a set of N Boltzmann equations,

$$\begin{aligned} \frac{dn_i}{dt} = -3Hn_i - \sum_{j,X} \big[& \langle \sigma_{ij} v \rangle \left(n_i n_j - n_i^{eq} n_j^{eq} \right) \\ & - \left(\langle \sigma'_{ij} v \rangle \, n_i n_X - \langle \sigma'_{ji} v \rangle \, n_j n_{X'} \right) \\ & - \Gamma_{ij} (n_i - n_i^{eq}) \big], \end{aligned} \tag{7}$$

where the n_X are number densities of the Standard Model particles involved in the interactions. Their nature will not be important, apart from the assumption that they are light enough that they are relativistic at freeze-out. The sum over X implies that

all relevant reactions are to be included. In Eq. (7) we have defined the cross sections and decay rates

$$\sigma_{ij} = \sigma(\chi_i \chi_j \to X X')$$
$$\sigma'_{ij} = \sigma(\chi_i X \to \chi_j X')$$
$$\Gamma_{ij} = \Gamma(\chi_i \to \chi_j X X').$$

The first term on the right of Eq. (7) is the dilution of number density due to the expansion of the Universe. The second term is due to both forward and backward reactions of type Eq. (6a). The third term is due to forward and backward reactions of type Eq. (6b), which only change n_i if $i \neq j$. The fourth term refers to decays and inverse decays, Eq. (6c).

Since all the χ_i which survive annihilation eventually decay into χ_1, the relevant quantity is the total density of χ_i particles, $n = \sum_{i=1}^{N} n_i$. Using Eq. (7) we find

$$\frac{dn}{dt} = -3Hn - \sum_{i,j=1}^{N} \langle \sigma_{ij} v \rangle \left(n_i n_j - n_i^{eq} n_j^{eq} \right). \tag{8}$$

A few subtleties regarding Eq. (8) should be pointed out. First we have implicitly assumed that the χ particles are scalars or Majorana fermions which can annihilate with themselves and do not have a cosmic asymmetry. The corresponding equations for Dirac fermions can be easily found. Second, since in reactions such as Eq. (6a) with $i = j$, two χ_i particles are lost, one might expect a factor of two in Eqs. (7) and (8) when $i = j$. However, a factor of $1/2$ occurs in the thermal average (due to identical particles) and so there is no factor of two. Lastly, note that the sum in Eq. (8) is over both i and j, and since σ_{ij} is symmetric there is effectively a factor of two in front of terms such as σ_{12}.

Next, we note that there is a huge quantitative difference in the rates of reactions of type Eq. (6a), as compared to those of type (6b) and (6c), at the temperatures relevant for freeze-out. The rate of a reaction of type (6a) is $n_i n_j \sigma_{ij} \sim T^3 m_i^{3/2} m_j^{3/2} \sigma_{ij} \exp(-(m_i + m_j)/T)$, while the rate for a reaction of type (6b) is $n_i n_X \sigma'_{ij} \sim T^{9/2} m_i^{3/2} \sigma'_{ij} \exp(-m_j/T)$. So the latter rates are larger by a factor of roughly $n_X/n_j \sim (T/m_j)^{3/2} \exp(m_i/T) \sim 10^9$, where the last relation follows from the fact that for a particle species to be a dark matter candidate the freeze out temperature will be roughly, $T_f \sim m_1/25$, and we have assumed that the cross sections σ_{ij} and σ'_{ij} are not radically different. Reactions of type (6c) may take place even faster than (6b), depending upon details of the kinematics. Since it is reactions of type Eq. (6a)

which determine the freeze-out (see Eq. (8)), this allows us to accurately approximate $n_i/n \approx n_i^{eq}/n^{eq}$, *i.e.* the ratio of χ_i density to total χ density maintains its equilibrium value before, during and after freeze-out. It is convenient then to define

$$r_i \equiv n_i^{eq}/n^{eq} = \frac{g_i(1+\Delta_i)^{3/2}\exp(-x\Delta_i)}{g_{eff}}, \tag{9}$$

where

$$\Delta_i = (m_i - m_1)/m_1,$$

and

$$g_{eff} = \sum_{i=1}^{N} g_i(1+\Delta_i)^{3/2}\exp(-x\Delta_i). \tag{10}$$

Using these definitions and the approximation $n_i/n \approx n_i^{eq}/n^{eq}$, Eq. (8) can be written in the form

$$\frac{dn}{dt} = -3Hn - \langle\sigma_{eff}v\rangle(n^2 - {n_{eq}}^2), \tag{11}$$

where

$$\begin{aligned}\sigma_{eff} &= \sum_{ij}^{N}\sigma_{ij}r_i r_j, \\ &= \sum_{ij}^{N}\sigma_{ij}\frac{g_i g_j}{g_{eff}^2}(1+\Delta_i)^{3/2}(1+\Delta_j)^{3/2}\exp -x(\Delta_i+\Delta_j).\end{aligned} \tag{12}$$

Eq. (11) is now in the form of the standard equation, Eq. (1) and can be solved using similar techniques, *i.e.* solving for x_f and performing the appropriate annihilation integral.

The freeze-out temperature, Eq. (2), is replaced by

$$x_f = \ln\frac{.038 g_{eff} m_{pl} m_1 \langle\sigma_{eff}v\rangle}{{g_*}^{1/2}x_f^{1/2}}. \tag{13}$$

We write the annihilation integral (Eq. (3)) in the form

$$J = (a_{11}I_a + 3b_{11}I_b/x_f)/x_f,$$

where

$$I_a = \frac{x_f}{a_{11}} \int_{x_f}^{\infty} x^{-2} a_{eff} dx$$
$$I_b = \frac{2x_f^2}{b_{11}} \int_{x_f}^{\infty} x^{-3} b_{eff} dx, \tag{14}$$

and, for comparison with the normal formulas, we have Taylor expanded the cross sections $\sigma_{ij} = a_{ij} + b_{ij}v^2$, and $\sigma_{eff} = a_{eff} + b_{eff}v^2$. The formulas for a_{eff} and b_{eff} are the same as Eq. (12) with σ_{ij} replaced by a_{ij} or b_{ij}. The corresponding formula for the relic abundance is then

$$\Omega h^2 = \frac{1.07 \times 10^9 x_f}{{g_*}^{1/2} m_{pl}(\mathrm{GeV})(a_{11} I_a + 3 b_{11} I_b / x_f)}, \tag{15}$$

which is the same as Eq. (5) except for the replacement of a_{11} with $a_{11} I_a$ and b_{11} with $b_{11} I_b$, and, of course, it must be evaluated at the new value of x_f.

We are now in a position to evaluate the relic abundance in several cases and discuss the effect of the heavier χ's. We compare to the result ignoring the heavier χ's by forming the ratio

$$R \equiv \Omega_{old}/\Omega_{new} \approx J_{new}(x_{f,new})/J_{old}(x_{f,old}). \tag{16}$$

First, we note that in the limit where the σ_{ij} are all equal, both the integrals I_a and I_b are unity, so, in this limit, the only change to the relic abundance comes from the change to the freeze-out temperature, where g_1 is replaced by g_{eff}. If, in addition, there is mass[10] and degree-of-freedom degeneracy, then $g_{eff} = N g_i$. This is just as expected, since in this limit the extra χ_i particles act precisely as extra degrees of freedom of the χ_1 particle. For particles with only s-wave annihilations, the change in relic abundance is given in this limit by $R \approx 1 - x_f^{-1} \ln N \approx 1 - .04 \ln N$. We see that for typical values of N (such as $N = 2$) this is less than a 5% effect. So just having extra particles near in mass to a dark matter candidate will not make a big difference as long as the cross sections are similar.

As the next example, consider the case of supersymmetry. Suppose that a squark ($\tilde{q}$) (χ_2 in our notation), the supersymmetric partner of a quark, exists with a mass near to that of the the LSP [which we will denote χ_1 and assume to be a photino ($\tilde{\gamma}$), or neutralino ($\tilde{\chi}$)]. In this case the cross sections σ_{ij} will *not* all be identical.

In fact, examination of the appropriate Feynman diagrams shows that one expects $\sigma_{22}(\tilde{q}\bar{\tilde{q}} \to gg) \simeq (\alpha_s/\alpha)\sigma_{12}(\tilde{\chi}\tilde{q} \to qg) \simeq (\alpha_s/\alpha)^2\sigma_{11}(\tilde{\chi}\tilde{\chi} \to q\bar{q})$, where g denotes a gluon, q denotes a quark, α_s is the strong interaction coupling and α is the electroweak coupling. Since $\alpha_s/\alpha \approx 20$, we will consider, as an example, a system of two particles ($N = 2$) with cross sections which do not depend on temperature (a terms only) and have the values $\sigma_{22} = A\sigma_{12} = A^2\sigma_{11}$, with $A \approx 20$. The effective cross section, Eq. (12), then becomes

$$\sigma_{eff} = \sigma_{11}\left(\frac{1+Aw}{1+w}\right)^2, \tag{17}$$

where $w = (1+\Delta)^{3/2}\exp(-x\Delta)g_2/g_1$, $\Delta = (m_2 - m_1)/m_1$, and $x = m_1/T$. The effective number of degrees of freedom becomes $g_{eff} = g_1(1+w)$. First consider the degenerate limit, $\Delta = 0$; then $\sigma_{eff}(deg) = \sigma_{11}(1 + Ag_2/g_1)^2/(1 + g_1/g_2)^2 \approx \sigma_{11}A^2/(1+g_1/g_2)^2$, and $R(deg) \approx I_a \approx A^2/(1+g_1/g_2)^2$. Thus for the case of a single degenerate squark we have $g_2/g_1 = 3$ and the relic abundance is smaller by a factor of about 200. If all six squark flavors and both left and right chiral states were degenerate, then $g_2/g_1 = 18$, and the final relic abundance of neutralinos would be smaller than previous calculations would indicate by a factor of around 350. We see that this can be a very substantial effect.

For non-degenerate masses we must return to the integrals of Eq. (14). In Fig. 1 we show the result of the numerical integration[11] for several relevant values of A, $x_{f,old}$ and g_2. Fig. 1a shows $A = 20$ and $g_2/g_1 = 3$, relevant if only one chiral state of one flavor of squark is light. Curves for scaled freeze-out temperatures of $x_{f,old} = 20$, 25, and 30 are shown. The actual value of $x_{f,old}$ depends upon the details of the neutralino composition and mass, but typically falls within this range.

The crosses in Fig. 1a show the result of numerically solving the Boltzmann equation, Eq. (11), for a cross section corresponding to $x_{f,old} = 25$, while the solid lines use the standard matching technique. It is clear that the standard technique gives good agreement with the numerical computation. This allays our fears about using the standard matching technique at freezeout, and we will herewith dispense with numerically integrating the Boltzmann equation. If one desires solutions of higher accuracy then such numerical integration must be done, but one should also include the refinements discussed in Section II.

Fig. 1b shows the effect of varying the co-annihilation cross section enhancement A, while Fig. 1c shows the effect of varying the number of co-annihilating species. The $g_2/g_1 = 18$ case is relevant when there are 6 light squarks. From these figures, one can decide how near in mass χ_2 must be for our co-annihilation effect to be important.

We see that a sizable effect on the relic abundance occurs as long as $\Delta < 0.1$, that is, as long as the second lightest particle is within around 10% of the lightest particle's mass. For values of A larger than 20, or when there are several co-annihilating degrees of freedom, mass differences of 15% or even 20% can be important.

We conclude that whenever additional particles exist within around 10% of the LSP mass, annihilations of the heavier particles cannot be ignored, and the techniques developed in this section should be used.

IV. Annihilation into "Forbidden" Channels

In this section we consider the case where a dark matter candidate is slightly below the mass threshold for annihilation and for which a substantial cross section would exist if the candidate were more massive. For example, suppose that $2m_1 \gtrsim m_{H_2} + m_{H_3}$, where m_1 is the mass of the LSP of supersymmetry (a photino or neutralino) and m_{H_2} and m_{H_3} are the masses of the Higgs bosons. It is known that when the channel $\chi\chi \to H_2H_3$ is open, it dominates the annihilation cross section by up to a factor of 500 and therefore determines the relic abundance.[12] In the standard treatment, this channel would not be considered when it was "forbidden" at zero relative velocity. However, since freeze-out occurs at a temperature $T_f \approx m_1/25$, and since the χ particles are Boltzmann distributed, the annihilation into heavier particles does take place at some rate. If the masses of the annihilation products are not too much greater, this kind of annihilation can dominate the cross section.

Before considering the forbidden case, it is useful to consider the case where annihilation occurs into an allowed channel but the mass of the final state particles is large enough so that it cannot be neglected. We will denote the relic particle by χ_1 and its mass by m_1. For simplicity we consider the case where both final state particles have the same mass, m_2. As stated earlier it is common practice to Taylor expand the cross-section[13] in the form $(\sigma v) = a + bv^2$. When the mass of the final state particles is small, so they are moving relativistically, this is fine; however, near kinematic thresholds this expansion breaks down and it is more appropriate to write the cross-section in the form $(\sigma v) = (a' + b'v^2)v_2$, where v_2 is the velocity of the final state particles in the center of mass frame. The factor of v_2 is always there,[14] it arises from doing the integral over the phase space of the outgoing particles, and is the reason the expansion blows up near thresholds.

Defining the mass ratio $z = m_2/m_1$ we write

$$\begin{aligned} v_2 &= (1 - z^2 + z^2v^2/4)^{1/2} \\ &= z(v^2/4 + \mu_+^2)^{1/2}, \end{aligned} \tag{18}$$

where $\mu_+ = \sqrt{1-z^2}/z$ is the minimum value of v_2, and as always $v = 2p_1/E_1$ is the "relative velocity" of the χ_1's in the center of mass frame. To approximate the effects of finite m_2, v_2 is often Taylor expanded in v^2

$$v_2 \approx (1-z^2)^{1/2}\left(1+\frac{z^2v^2}{8(1-z^2)}\right), \tag{19}$$

however, very near threshold this formula is clearly inadequate since then $z \to 1$, and the 'small' term in the expansion becomes infinite. Therefore, when calculating cross sections and relic abundances near a threshold, it is essential to keep the factor of v_2 without approximation. The thermally averaged cross-section above threshold ($z < 1$, or "allowed"), is

$$\langle \sigma v \rangle_{all} = \left\langle (a' + b'v^2)v_2 \right\rangle = \frac{x^{3/2}}{2\pi^{1/2}} \int_0^\infty dv v^2 e^{-v^2x/4} v_2 (a' + b'v^2) \tag{20}$$

and after a change of variables, $t = v^2x/4$,

$$\langle \sigma v \rangle_{all} = \frac{2z}{\pi^{1/2}} \int_0^\infty (t/x + \mu_+^2)^{1/2} t^{1/2} \left(a' + 4b't/x\right) e^{-t} dt, \tag{21}$$

Similar formulas may be written when m_1 is below threshold ($z > 1$ or "forbidden"). In thermally averaging the cross section, we now integrate from $v = v_c$ to $v = \infty$, where $v_c = 2\mu_- = 2(1 - m_1^2/m_2^2)^{1/2}$ is the critical velocity to activate the reaction. The analogous formula to Eq. (20) is

$$\langle \sigma v \rangle_{for} = \left\langle (a' + b'v^2)v_2 \right\rangle = \frac{x^{3/2}}{2\pi^{1/2}} \int_{2\mu_-}^\infty v_2 (a' + b'v^2) v^2 e^{-v^2x/4} dv. \tag{22}$$

Now we change variables to $t = v^2x/4 - \mu_-^2 x$, and find

$$\langle \sigma v \rangle_{for} = e^{-\mu_-^2 x} \frac{2z}{\pi^{1/2}} \int_0^\infty (t/x + \mu_-^2)^{1/2} t^{1/2} \left[(a' + 4b'\mu_-^2) + 4b't/x\right] e^{-t} dt, \tag{23}$$

where $\mu_- = (z^2-1)^{1/2}/z$. Apart from the factor of $e^{-\mu_-^2 x}$, a change from μ_+ to μ_-, and the $4b'\mu_-^2$ term, Eq. (23) is identical to Eq. (21). At threshold ($\mu_+^2 = \mu_-^2 = 0$ or

$z = 1$) the formulas are identical, and a simple integration leads to

$$\left\langle (a' + b'v^2)v_2 \right\rangle_{z=1} = \frac{2}{\pi^{1/2} x^{1/2}} \left[a' + 8b'/x \right]. \tag{24}$$

Near freezeout, $x_f \approx 25$, the s-wave annihilation is suppressed at threshold by a factor of about .25, but it does not vanish, nor does it blow up. Similarly, the p-wave cross-section is suppressed by a factor of $\approx .30$ from its value at $z = 0$.

In general, Eqs. (21) and Eq. (23) may be evaluated numerically, but for the case of an s-wave cross section ($b' = 0$) the integral may be done analytically

$$\left\langle a' v_2 \right\rangle = a' \frac{\mu_\pm^2 z x^{1/2}}{\pi^{1/2}} e^{\pm \mu_\pm^2 x/2} K_1(\mu_\pm^2 x/2), \tag{25}$$

where K_1 is a modified Bessel function. Far from threshold ($\mu_\pm^2 \to \infty$) the Bessel function is approximated by $K_1(\mu_\pm^2 x/2) \sim \sqrt{\frac{\pi}{\mu_\pm^2 x}} e^{-\mu_\pm^2 x/2}$, and the thermal averages reduce to

$$\left\langle a' v_2 \right\rangle \approx \begin{cases} a'\mu_+ z = a'\sqrt{1-z^2}, & m_1 \gg m_2 \\ a'\mu_- z e^{-\mu_-^2 x}, & m_1 \ll m_2. \end{cases}$$

The first relation contains the usual $\sqrt{1-z^2}$ correction for the mass of the final state particle. At threshold, $z \to 1$, $\mu_\pm \to 0$, the Bessel function is given by $K_1(\mu_\pm^2 x/2) \approx 2/(\mu_\pm^2 x)$, and the thermal average is $\langle a' v_2 \rangle \approx 2a'/(\pi x)^{1/2}$, as before.

Unfortunately, placing the thermally averaged cross section in the form of Eq. (25) is not all that useful since to calculate the relic abundance one must still perform the annihilation integrals. Although these can be done numerically, various expansions for $\langle \sigma v \rangle$ allow approximate analytic results. For large $\mu_\pm^2 x$, an asymptotic expansion can be performed. Above threshold this gives the familiar result,

$$\left\langle (a' + b'v^2)v_2 \right\rangle_{all} \approx (1-z^2)^{1/2} \left[a'(1 + \frac{3z^2}{4x(1-z^2)}) + \frac{6b'}{x}(1 + \frac{5z^2}{4x(1-z^2)}) \right], \tag{26}$$

and in the deeply forbidden region,

$$\begin{aligned} \left\langle (a' + b'v^2)v_2 \right\rangle_{for} \approx z\mu_- \exp(-\mu_-^2 x) \big[& a'(1 + \frac{3}{4\mu_-^2 x}) \\ & + 4b'\mu_-^2 (1 + \frac{9}{4\mu_-^2 x} + \frac{45}{32\mu_-^4 x^2}) \big]. \end{aligned} \tag{27}$$

Very near threshold we expand in $\mu_\pm^2 x \ll 1$,

$$\left\langle (a' + b'v^2)v_2 \right\rangle_{thr} \approx \frac{2z}{\pi^{1/2}x^{1/2}} \left[a'(1 - x\Delta) + \frac{8b'}{x}(1 - \frac{x\Delta}{2}) \right], \tag{28}$$

where $\Delta = z - 1 = (m_2 - m_1)/m_1$ is the fractional mass excess of the final state particles.

The three approximate results, as well as the numerical integration are shown in Fig. 2 for $x = 25$. Fig. 2a shows a "pure s-wave" annihilation ("a'" terms only) results, while Fig. 2b shows a "p-wave" ("b'" terms only) annihilation. The problem at $z = 1$ for the usual (allowed) approximation is evident, as is the error caused by the standard approximation $\langle \sigma v \rangle = 0$, for $z \geq 1$. Far from threshold the expansions work well; however, near threshold one is advised to use Eq. (28). More exactly, the best piecewise (pw) approximation for s-wave annihilation is

$$\langle \sigma v \rangle_{a,pw} = \begin{cases} \langle \sigma v \rangle_{all}, & x\Delta < -.023 \\ \langle \sigma v \rangle_{thr}, & -.023 < x\Delta < .023 \\ \langle \sigma v \rangle_{for}, & .023 < x\Delta. \end{cases} \tag{29a}$$

and for p-wave annihilation

$$\langle \sigma v \rangle_{b,pw} = \begin{cases} \langle \sigma v \rangle_{all}, & x\Delta < -.046 \\ \langle \sigma v \rangle_{thr}, & -.046 < x\Delta < .023 \\ \langle \sigma v \rangle_{for}, & .023 < x\Delta. \end{cases} \tag{29b}$$

The vertical lines in Fig. 2 mark the transition values.

Using the various results for the thermally averaged cross-sections, the relic abundance can be calculated from Eqs. (3) and (4) as described in Section II. To compare with the standard results, we will explicitly separate out the "forbidden" channel from the ordinary (*i.e.* $\chi_1\chi_1 \to XX$) channels,

$$(\sigma v)_{tot} = a_{11} + b_{11}v^2 + \left[(a' + b'v^2)v_2 \right], \tag{30}$$

where $(a' + b'v^2)v_2$ is the forbidden piece and $a_{11} + b_{11}v^2$ is the ordinary piece. The annihilation integral may be written as

$$J = (a_{tot} + 3b_{tot}/x_f)/x_f,$$

where x_f is the new value of x_f computed by iteratively using $(\sigma v)_{tot}$ and Eq. (2). The quantities a_{tot} and b_{tot} also contain an explicit separation of the forbidden and

ordinary channels: $a_{tot} = a_{11} + a' I'_a$, $b_{tot} = b_{11} + b' I'_b$, where we define

$$\begin{aligned} I'_a &= \frac{x_f}{a'} \int_{x_f}^{\infty} \langle a' v_2 \rangle \, x^{-2} dx \\ I'_b &= \frac{2x_f^2}{b'} \int_{x_f}^{\infty} \frac{\langle b' v^2 v_2 \rangle}{6} x^{-2} dx. \end{aligned} \tag{31}$$

Using Eq. (28) near threshold ($z \approx 1$), we have

$$\begin{aligned} I'_{a,thr} &\approx \frac{4z}{3\pi^{1/2} x_f^{1/2}} (1 - 3x_f \Delta) \\ I'_{b,thr} &\approx \frac{32z}{15\pi^{1/2} x_f^{1/2}} (1 - \frac{5}{6} x_f \Delta) \end{aligned} \tag{32}$$

For the forbidden region ($z > 1$) we use Eq. (27) and evaluate the integral in Eq. (31) by asymptotic expansion to find

$$\begin{aligned} I'_{a,for} &\sim \frac{z}{\mu_- x_f} e^{-\mu_-^2 x_f} \\ I'_{b,for} &\sim \frac{4}{3} z \mu_- e^{-\mu_-^2 x_f} \left(1 + \frac{1}{4\mu_-^2 x_f} \right). \end{aligned} \tag{33}$$

where the behavior near $z = 1$ has dictated the number of terms kept in the expansion. Above threshold ($z < 1$), the non-relativistic expansion gives

$$\begin{aligned} I'_{a,all} &\approx (1 - z^2)^{1/2} \left(1 + \frac{3z^2}{8(1 - z^2) x_f} \right) \\ I'_{b,all} &\approx (1 - z^2)^{1/2} \left(1 + \frac{5z^2}{6(1 - z^2) x_f} \right). \end{aligned} \tag{34}$$

Far above threshold ($z \ll 1$) we see that $I'_a \approx I'_b \approx 1$ and we recover the standard result. Note that while previous calculations would have predicted no effect on relic abundance for annihilation at threshold, Eq. (32) shows an effect of 15% of the $z \ll 1$ limit for s-wave annihilation and a 25% effect for p-wave annihilation (for $x_f = 25$).

We now discuss the values of Δ for which "forbidden" channel annihilation may be significant. First consider the case of "pure s-wave" annihilation. We define the annihilation cross-section into massless particles as $(\sigma v) = a_{11}$ and the forbidden channel cross section as $(\sigma v)_{for} = a' v_2$. We characterize the strength of the forbidden channel by $a' = A' a_{11}$, *i.e.* A' is the factor by which the forbidden annihilation would dominate the cross section if it were not kinematically suppressed. Recall that for the previously mentioned example of neutralinos annihilating into Higgs bosons $A' \sim 50 - 500$. Large values of A' can also arise for other channels such as top quarks or W^+W^-.

In Fig. 3, we plot the resulting decrease in relic abundance for $x_{f,old} = 25$. Fig. 3a shows the reduction in Ω for "pure s-wave" annihilation (a' terms only), where $R = \Omega_{old}/\Omega_{new} = (1 + A' I'_a) x_{f,old}/x_{f,new}$, and in Fig. 3b we show the result for "pure p-wave" annihilation (b' terms only), where $R = (1 + A' I'_b) x^2_{f,old}/x^2_{f,new}$. The solid curves show the results of performing the integrals for $\langle \sigma v \rangle$ numerically for $A' = 20$, 100, and 500. For $A' = 500$ we also show both of the asymptotic expansion approximations as well as the threshold approximation for appropriate ranges of $x_f \Delta$. Unfortunately, no approximation is particularly good for s-wave annihilation in the interesting range $.01 \lesssim x_f \Delta \lesssim .05$. As an alternative to the full double integral performed for the solid curves, we have evaluated the annihilation integral numerically using the piecewise cross-sections of Eq. (29). The result is shown as the dot-dashed curve. The agreement between the dot-dashed curve and the $A' = 500$ solid curve is better than 10%.

We see from Fig. 3 that, depending on A', new channels are important even when the masses are 10%-15% below threshold. We conclude that if $\Delta < 0.05$–0.1 and the unsuppressed "forbidden" cross section is more than 10 times larger than the "allowed" cross section, this effect is important. For the example of neutralino annihilation into Higgs bosons discussed earlier, an enhancement of between 50 and 500 is typical[12] and so this channel should be included at neutralino masses of 10–15% *below* the $v = 0$ kinematic threshold. We also note that above threshold, the usual Taylor series expansion is adequate until $\Delta \gtrsim -.02$.

V. Annihilation near poles

In this section we consider the case where the non-relativistic annihilation, which determines the relic abundance, takes place near a pole in the cross section. This can occur, for example, when there is s-channel exchange of a Z-boson or scalar particle. A pole can also occur when the annihilating dark matter particle is nearly one-half the mass of a resonance such as the J/Ψ, η, or Υ particle. These cases have been treated

in the literature using various approximations, all of which give substantial errors near the pole.[4]

For our example we will consider a cross section

$$\sigma v = \frac{\alpha^2 s}{(M_{ex}^2 - s)^2 + M_{ex}^2 \Gamma_{ex}^2}, \tag{35}$$

where $\alpha \approx .01$ is the square of some coupling constant, M_{ex} is the mass of the exchanged particle, Γ_{ex} is the total width of the exchanged particle, $s = 4m_1^2/(1 - v^2/4)$ is the Mandelstam variable, m_1 is the mass of the dark matter particle, and v is as usual the "relative velocity". This cross section is modeled after s-channel Z exchange, but the techniques we describe can be applied to other types of poles as well.

In order to present our results in a more universal way we will use the scaled variables

$$u = \left(\frac{2m_1}{M_{ex}}\right)^2 \qquad \text{and} \qquad \epsilon = \left(\frac{\Gamma_{ex}}{M_{ex}}\right)^2. \tag{36}$$

The cross section becomes

$$\sigma v = \frac{\alpha^2 u/(1 - v^2/4)}{M_{ex}^2[(1 - u/(1 - v^2/4))^2 + \epsilon]}. \tag{37}$$

At zero relative velocity the pole occurs at $u = 1$, while in general it occurs at $u_p = 1 - v_p^2/4$, or $v_p = 2(1 - u_p)^{1/2}$. The value of our cross section at the pole is $(\sigma v)_{pole} = \alpha^2/(M_{ex}^2 \epsilon)$.

The earliest treatments of relic abundances concentrated on light dark matter particles and used effective 4-fermion interactions which ignored poles altogether. This is, of course, completely inadequate when a pole is present. For the Z resonance $\epsilon_Z \approx 7.5 \times 10^{-4}$ and the peak cross section is therefore very much larger than the cross section away from the pole. For resonances such as the J/Ψ, η, or Υ the cross sections are even more peaked since $\epsilon_\Psi \approx 4.8 \times 10^{-10}$, $\epsilon_\eta \approx 3.7 \times 10^{-6}$, and $\epsilon_\Upsilon \approx 3.0 \times 10^{-11}$, but in these cases the cross sections are not quite of the form Eq. (37) and a modified treatment is needed.

For use in relic abundance calculations the cross section must be thermally averaged. The standard method is to Taylor expand it to first order in v^2 and then substitute $\langle v^2 \rangle = 6/x$, where $x = m_1/T$ as usual. However, for small ϵ, the expansion in v^2 breaks down near the pole and the standard method gives extremely poor results, even allowing the cross section to become negative in the case of Eq. (37). While some

authors have used this Taylor expansion method near poles, a more common approach has been to factor off the pole factor $P(v^2) = \left([1 - u/(1 - v^2/4)]^2 + \epsilon\right)^{-1}$ before making the Taylor expansion, and then multiply the result by the pole factor at zero relative velocity. For our example cross section this would give an approximation to the thermally averaged cross section of

$$\langle \sigma v \rangle_0 = \frac{\alpha^2 u}{M_{ex}^2}(1 + \frac{3}{2x})P(0), \tag{38}$$

where the $3/2x$ term comes from the thermal average of $\langle v^2/4 \rangle$ in Eq. (37). (It is actually superfluous for our purposes.) Another possibility is to approximate $\langle \sigma v \rangle$ by just substituting $v^2 \to 6/x$ in σv. This gives the correct expansion far from the pole and moves the peak away from $v = 0$ and closer to where one might think it belongs.

$$\langle \sigma v \rangle_{subs} = (\sigma v)_{v^2 = 6/x}. \tag{39}$$

The main point of this section is to show that all of these approximations are quite unreliable near a pole when ϵ is small. In Fig. 4 we plot a numerical evaluation of $\langle \sigma v \rangle$ as a function of u and compare it with the Taylor expansion, $\langle \sigma v \rangle_0$, and $\langle \sigma v \rangle_{subs}$. The numerical $\langle \sigma v \rangle$ is found from

$$\langle \sigma v \rangle_{num} = \frac{x^{3/2}}{2\pi^{1/2}} \int_0^\infty dv v^2 (\sigma v) e^{-xv^2/4}. \tag{40}$$

In Fig. 4a we show the comparison for $\epsilon = 7.5 \times 10^{-4}$, $M_{ex} = 91$ GeV $\alpha = 0.01$ and $x = 25$, corresponding roughly to a pole due to Z boson exchange. Note that if this were the Z pole the limits of the plot would correspond to $\sqrt{u} = .6$ or $m_1 = 27.3$ GeV and $\sqrt{u} = 1.2$ or $m_1 = 54.6$ GeV. Although the Taylor expansion does reasonably well for $m_1 < M_{ex}$, it does very poorly (even producing a negative cross-section) for $m_1 > M_{ex}$. For the Z pole, the $\langle \sigma v \rangle_{subs}$ approximation does slightly better than the $\langle \sigma v \rangle_0$ approximation away from the pole, but neither puts the pole in the right place. The numerical results differ in places from both approximations by more than a factor of 3. Fig. 4b shows the same for a deeper pole, $\epsilon = 10^{-6}$. In this case the disagreements between the approximations and the numerical integration are even more striking. Here the approximations give poles which are much too narrow and much too strongly peaked and differ greatly from the numerical results over a wide range of masses.

Note, however, that even in Eq. (40) at least two approximations are being made. First we are assuming that x is large enough so that $\exp(-xv^2/4)$ is very small before v approaches its maximum (relativistic) value of 2. Second we are averaging in the center-of-mass system, which as pointed out by Srednicki, Watkins, and Olive,[3] is not completely correct. Since in the pole case, the cross section has a dependence on v^2 which is non-polynomial, and only polynomial dependence has been previously tested, we might worry that these approximations introduce errors larger than our 10-20% criteria. To check that the approximations in Eq. (40) are valid, we can perform numerically the three-dimensional integral given in Ref. 3 (their Eq. (26)). In Fig. 5 we show a comparison of the numerical evaluation of Eq. (40) and a numerical evaluation of the three-dimensional integral. As shown by the figure, the two methods agree quite well, differing in general by less than 20%. Some of the differences which do occur may, in fact, be due to the numerical integration routine, which has trouble performing three-dimensional integrals of very sharply peaked functions. We will from now on use Eq. (40). In a case where maximum accuracy is important, Eq. (40) should be replaced with Eq. (26) of Ref. 3 as discussed in Section II. Note that the expansion given in Ref. 3 should *not* be used since it has the same problems near a pole as the Taylor expansion in v^2, and therefore is more unreliable than the simple approximations discussed above.

Returning to Fig. 4, we can understand the discrepancies between the simple approximations and the numerical evaluation by examining Eq. (40). This formula for the thermal average results in a "weighted" area under the cross section peak, while both approximations just use the height of the peak as the average. For small ϵ and $u < 1$, one sees that the integral is dominated by the area under the peak and, in fact, can be approximated by expanding about the peak ($v_p = 2(1-u)^{1/2}$ for $u < 1$). Changing variables to $\nu = v - v_p$, where ν is small, we can approximate $u/(1-v^2/4) \approx 1 + \nu(1-u)^{1/2}/u$ and approximate the thermal average integral as

$$\langle \sigma v \rangle \approx \frac{x^{3/2}}{2\pi^{1/2}} v_p^2 e^{-xv_p^2/4} \frac{\alpha^2}{M_{ex}^2} \int_{-\nu_0}^{\nu_0} \frac{d\nu}{[\nu^2(1-u)/u^2] + \epsilon}, \tag{41}$$

where $\nu_0 \ll v_p$ defines a small interval around the peak. The integral above can be evaluated (for $u < 1$)

$$\int_{-\nu_0}^{\nu_0} \frac{d\nu}{[\nu^2(1-u)/u^2] + \epsilon} = \frac{2u}{\sqrt{\epsilon(1-u)}} \tan^{-1}\left(\nu_0 \sqrt{\frac{1-u}{\epsilon u^2}}\right). \tag{42}$$

If $\sqrt{\epsilon}$ is small compared to $\nu_0\sqrt{1-u}$ the inverse tangent can be approximated as $\pi/2$,

independent of ν_0. Comparing the resulting formula for $\langle\sigma v\rangle$ with the maximum cross section $(\sigma v)_{pole} = \alpha^2/(\epsilon M_{ex}^2)$, we find

$$r_\sigma = \frac{\langle\sigma v\rangle}{(\sigma v)_{pole}} \approx 2\sqrt{\pi}x^{3/2}u\sqrt{\epsilon}(1-u)^{1/2}e^{-x(1-u)}. \tag{43}$$

Finally taking $\sqrt{u} \approx .98$ as the rough position of the thermally averaged pole, with $x \approx 25$, we find $r_\sigma \approx 31\sqrt{\epsilon}$. For $\epsilon = 10^{-6}$ this gives $r_\sigma \approx 0.03$ just as shown in Fig. 4b. For $\epsilon = 7.5 \times 10^{-4}$, the inequalities $\sqrt{\epsilon} \ll \nu_0\sqrt{1-u}$ and $\nu_0 \ll v_p$ are not satisfied for reasonable values of ν_0, so we must include the inverse tangent term. Choosing $\nu_0 \approx .1$ we find $r_\sigma \approx .37$, again in agreement with the curve in Fig. 4a. In general, for ϵ small enough so that the answer is independent of ν_0, Eq. (43) gives a good approximation near the pole (for $u < 1$). This approximation is shown in Fig. 4b as the long-dash curve. For larger ϵ, the approximations made in deriving Eq. (41) are no longer valid.

We have been discussing $\langle\sigma v\rangle$ but are actually interested in the relic abundance $\Omega_1 h^2$, for which we must evaluate the annihilation integral, Eq. (3). Here we find it useful to rewrite Eq. (3) as an explicit double integral over x and v, one of which may be easily performed,

$$J = \int_0^\infty dv \frac{v^2(\sigma v)}{\sqrt{4\pi}} \int_{x_f}^\infty dx x^{-1/2} e^{-xv^2/4} = \int_0^\infty dv v(\sigma v)\mathrm{erfc}(v\sqrt{x_f}/2). \tag{44}$$

In Eq. (44), (σv) is the *unaveraged* cross section and erfc is the complementary error function. Note that this formula is quite general and can be used in all cases to find the J integral. For σv of the form $a + bv^2$, Eq. (44) gives the standard result of Eq. (5), but for our pole cross section it must be performed numerically (or expanded about the pole as per Eq. (41)).

In Fig. 6 we plot the relic abundance which results from an iterative solution of the freeze-out equation and a numerical evaluation of Eq. (44). For comparison we show the results obtained using the two approximations for $\langle\sigma v\rangle$ described earlier. In particular, the approximations give $J_0 = (\alpha^2 u/M_{ex}^2)(1 + 3/(4x_f))P(0)/x_f$ for Ω_0 and $J_{subs} \approx \langle\sigma v\rangle_{subs}(1 - 3/(4x_f))/x_f$ for Ω_{subs}. Fig. 6a shows $\epsilon = 7.5 \times 10^{-4}$ and Fig. 6b shows $\epsilon = 10^{-6}$. While the approximations do better here than for $\langle\sigma v\rangle$, we still find that they give results off by up to a factor of three in the case of a Z-like pole and by several orders of magnitude for $\epsilon = 10^{-6}$.

We can again find an analytic understanding of the results shown in the figure by expanding about the pole. We find (for $u < 1$)

$$J \approx \frac{4\alpha^2}{M_{ex}^2}\frac{u}{\sqrt{\epsilon}}\mathrm{erfc}(\sqrt{x_f(1-u)})\tan^{-1}\left(\nu_0\sqrt{\frac{1-u}{\epsilon u^2}}\right), \tag{45}$$

where the inverse tangent can be taken as $\pi/2$ when $\sqrt{\epsilon} \ll \nu_0\sqrt{1-u}$. The resulting value of Ω is shown for $\epsilon = 10^{-6}$ ($u < 1$ only) as the long-dash curve in Fig. 6b. Again it is a good approximation near the pole for small ϵ. As before, for $\epsilon = 7.5 \times 10^{-4}$, it does not do as well. For small ϵ, the reduction in Ω can be extimated using

$$r_\Omega = \frac{\Omega}{\Omega_{pole}} = \frac{J_{pole}}{J} \approx \left[2\pi\epsilon^{1/2}ux_f\mathrm{erfc}\left(\sqrt{x_f(1-u)}\right)\right]^{-1}, \tag{46}$$

where $J_{pole} \approx \alpha^2 u_p/(M_{ex}^2 \epsilon x_f)$, and Ω_{pole} is the relic abundance at the peak of the pole.

In conclusion, we find that while the standard Taylor expansion in v^2 gives reasonable results away from pole regions, whenever dark matter annihilation takes place near a pole, special care must be taken, especially if results accurate to within a factor of two are desired. While we considered only one type of pole structure, we see that in general, narrow resonances in the cross section do not survive the thermal averaging and annihilation integration, giving features in the relic abundance curves which are broader and more shallow than naively expected.

Acknowledgments

We would like to thank R. Esmailzadeh, G. Gelmini, M. Kamionkowski, and E. W. Kolb for interesting discussions. This work was supported in part by the office of Science and Technology Centers of the NSF, under cooperative agreement AST-8809616, and by the DOE under grant DE-AC02-78ER05007.

REFERENCES

1. E. W. Kolb and M. S. Turner, *The Early Universe* (Addison-Wesley, Redwood City, 1989).
2. M. I. Vysotskil, A. D. Dolgov and Ya. B. Zeldovich, *J.E.T.P. Lett.* **26** 188 (1977); P. Hut, *Phys. Lett.* **69B** 85 (1977); K. Sato and M. Kobayashi, *Prog. Theor. Phys.* **58** 1775 (1977); B. W. Lee and S. Weinberg, *Phys. Rev. Lett.* **39** 165 (1977); D. A. Dicus, E. W. Kolb and V. L. Teplitz, *Phys. Rev. Lett.* **39** 168 (1977); G. Steigman, *Ann. Rev. Nucl. Part. Sci.* **29** 313-338 (1979); J. Bernstein, L. S. Brown and G. Feinberg, *Phys. Rev.* **D32** 3261 (1985); E. W. Kolb and K. A. Olive, *Phys. Rev.* **D33** 1202 (1986)
3. M. Srednicki, R. Watkins and K. A. Olive, *Nucl. Phys.* **B310** 693 (1988).
4. That poles should not be as sharp and deep as the simple approximations suggest has also been realized by E. W. Kolb (private communication) and by G. Gelmini and E. Roulet (private communication).
5. Except where otherwise noted, we will throughout average in the center-of-mass frame using the non-relativistic approximation, even though as shown by Srednicki, Watkins, and Olive,[3] this is not quite correct. More exact answers can be be found throughout by replacing our one dimensional integral with the three-dimensional integral given in their Eq. (26). The difference between the two methods is typically less than 10%, and in many cases much less.
6. At present the Hubble parameter is not known to a factor of two, which renders detailed ($\pm 10\%$) discussions of Ω rather moot; however, it is still important to avoid large errors such as discussed in this paper. We look forward to a day when h is well determined and the finer points of relic abundance calculations become important.
7. In our treatment we are ignoring the slight difference between the effective degrees of freedom defined by the energy density and the effective degrees of freedom defined by the entropy density, as well as the effect of changing degrees of freedom. For a more accurate treatment see, K. Griest and D. Seckel, *Nucl. Phys.* **B283,** 681 (1987); **B296,** 1034 (E) (1988).
8. R. J. Scherrer and M. S. Turner, *Phys. Rev* **D33** 1585 (1986).
9. K. Griest and M. Sher, *Phys. Rev. Lett.* **64,** 64 (1990); K. Griest and M. Sher, preprint CfPA-TH-90-002 (1990), to appear in *Phys. Rev.* D.
10. The relic abundance of particles in the degenerate limit was worked out simultaneously by R. Esmailzadeh and N. Tetradis (private communication).

11. For large Δ and large A ($A\exp(-x_f\Delta) \gg 1$ and $x_f\Delta \gg 1$) the integral can be done approximately using an asymptotic expansion, but the result ($I_a \sim 1 + 2Aw/(x_f\Delta)$) does not agree well with the numerical integration except for very large Δ.
12. K. Griest, M. Kamionkowski, and M. S. Turner, *Phys. Rev.* **D41,** 3565 (1990); G. Gelmini, P. Gondolo, and E. Roulet, preprint UCLA/90/TEP/5 (1990).
13. We caution that we have dropped the v^4 and higher terms, which will, of course, exist. Some of the results in the section include accuracy in the treatment of the v^0 and v^2 terms which is comparable to the error introduced by dropping the v^4 term.
14. Some authors implicitly Taylor expand v_2 and include the effects of finite mass in the coefficients a and b. To adapt our results to these papers requires a redefinition of a and b.

FIGURE CAPTIONS

1. Decrease in relic abundance due to co-annihilation. The decrease in relic abundance, $R = \Omega_{old}/\Omega_{new}$, is plotted *vs.* the mass splitting Δ for several cases. In (a) the cross section enhancement is $A = 20$ and $g_2/g_1 = 3$, relevant for the case of one light squark. Curves are shown for several relevant values of scaled freeze-out temperature $x_{f,old}$. For comparison, the crosses show the result of a numerical solution of the Boltzmann equation for a cross section equivalent to $x_{f,old} = 25$. In (b), the effect of varying the enhancement $A = \sigma_{12}/\sigma_{11}$ is shown. In (c) the effect of varying the number of co-annihilating species g_2 is shown. The curve for $g_2/g_1 = 18$ is relevant for 6 light squarks.
2. Cross section for annihilation into a "forbidden" channel. The thermal average of the cross section is shown for a "pure s-wave" (a) and a "pure p-wave" (b) cross section as defined in the text. The solid line is the result of a numerical integration and the dashed lines are the approximations A: $\langle\sigma v\rangle_{all}$, T: $\langle\sigma v\rangle_{thr}$, and F: $\langle\sigma v\rangle_{for}$, where the mass of the relic particle is respectively above, near and below threshold for annihilation into the forbidden channel. The best piecewise continuation is also indicated.
3. Decrease in relic abundance due to annihilation into a "forbidden" channel. The solid lines show the results of numerically evaluating the abundance for cross-section enhancements of $A' = 20$, 100, and 500. For $A' = 500$, the dot-dash line shows the result of using the piecewise cross-section, $\langle\sigma v\rangle_{pw}$, to evaluate the annihilation integral. The use of $\langle\sigma v\rangle_{pw}$ results in less than a 10% error.

The dashed lines show the three analytic approximations A: I_{all}, T: I_{thr}, and F: I_{for}. In (a) and (b) we show the results for "pure s-wave" and "pure p-wave" annihilation, respectively, for $x_{f,old} = 25$.

4. Thermal average of annihilation cross section near a pole. The solid curves show the numerical integration $\langle\sigma v\rangle_{num}$ (Eq. (40)) while the two short-dash curves show the commonly used approximations $\langle\sigma v\rangle_0$ (Eq. (38)), and $\langle\sigma v\rangle_{subs}$ (Eq. (39)). The $\langle\sigma v\rangle_0$ curve peaks at $\sqrt{u} = 1$, while the $\langle\sigma v\rangle_{subs}$ curve peaks at $\sqrt{u} < 1$. The dot-dash curve shows the Taylor expansion, which goes negative for a while. Parameter values $x = 25$, $M_{ex} = 91$ GeV, and $\alpha = .01$ were chosen. The units of the abscissa are GeV^{-2}. In (a) we set $\epsilon = 7.5 \times 10^{-4}$, roughly approximating a pole from Z boson exchange. In (b) we set $\epsilon = 10^{-6}$. The long-dash curve in (b) is our new approximation, Eq. (43).

5. Comparison of numerically performed thermal averages. The solid curve shows $\langle\sigma v\rangle_{num}$ (Eq. (40)), which uses the center-of-mass, and non-relativistic approximations. The crosses show the three-dimensional integral of Ref. 3. The same value of parameters were used as in Fig. 4a.

6. Relic abundance near a pole. The solid curves show the result of proper thermal averaging and integration of the Boltzmann equation, while the two short-dash curves show the commonly used approximations $\langle\sigma v\rangle_0$ with J_0, and $\langle\sigma v\rangle_{subs}$ with J_{subs}. The $\langle\sigma v\rangle_0$ curve bottoms at $\sqrt{u} = 1$, while the $\langle\sigma v\rangle_{subs}$ curve bottoms at $\sqrt{u} < 1$. Parameter values $x_{f,old} = 25$, $M_{ex} = 91$ GeV, and $\alpha = .01$ were chosen. In (a) we set $\epsilon = 7.5 \times 10^{-4}$, roughly approximating a pole from Z boson exchange. In (b) we set $\epsilon = 10^{-6}$. The long-dash curve in (b) uses the approximation, Eq. (43) and Eq. (46).

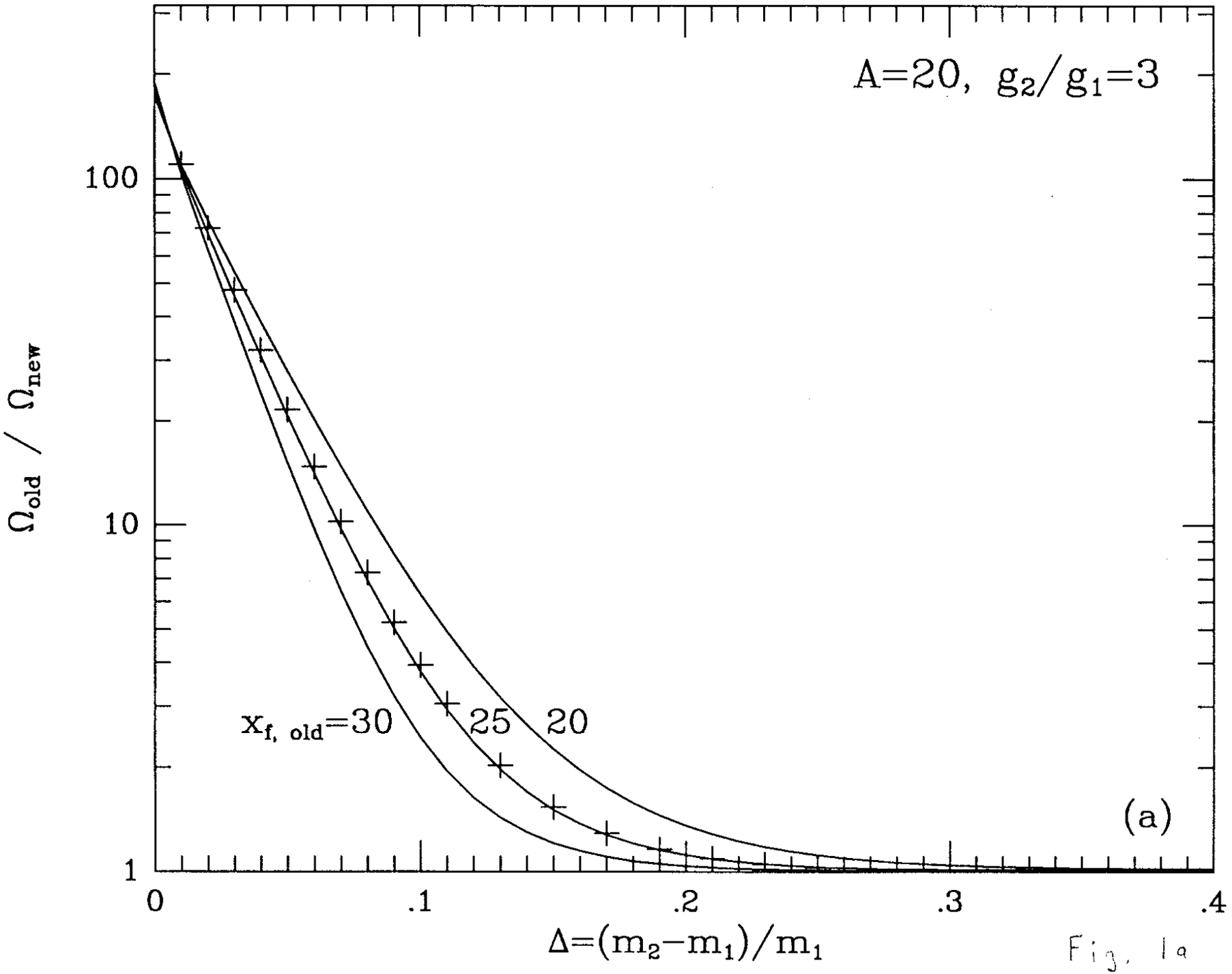
A=20, g_2/g_1=3
100
10
1
Ω_{old} / Ω_{new}
$x_{f,\ old}$=30
25
20
(a)
0
.1
.2
.3
.4
$\Delta=(m_2-m_1)/m_1$

Fig. 1a

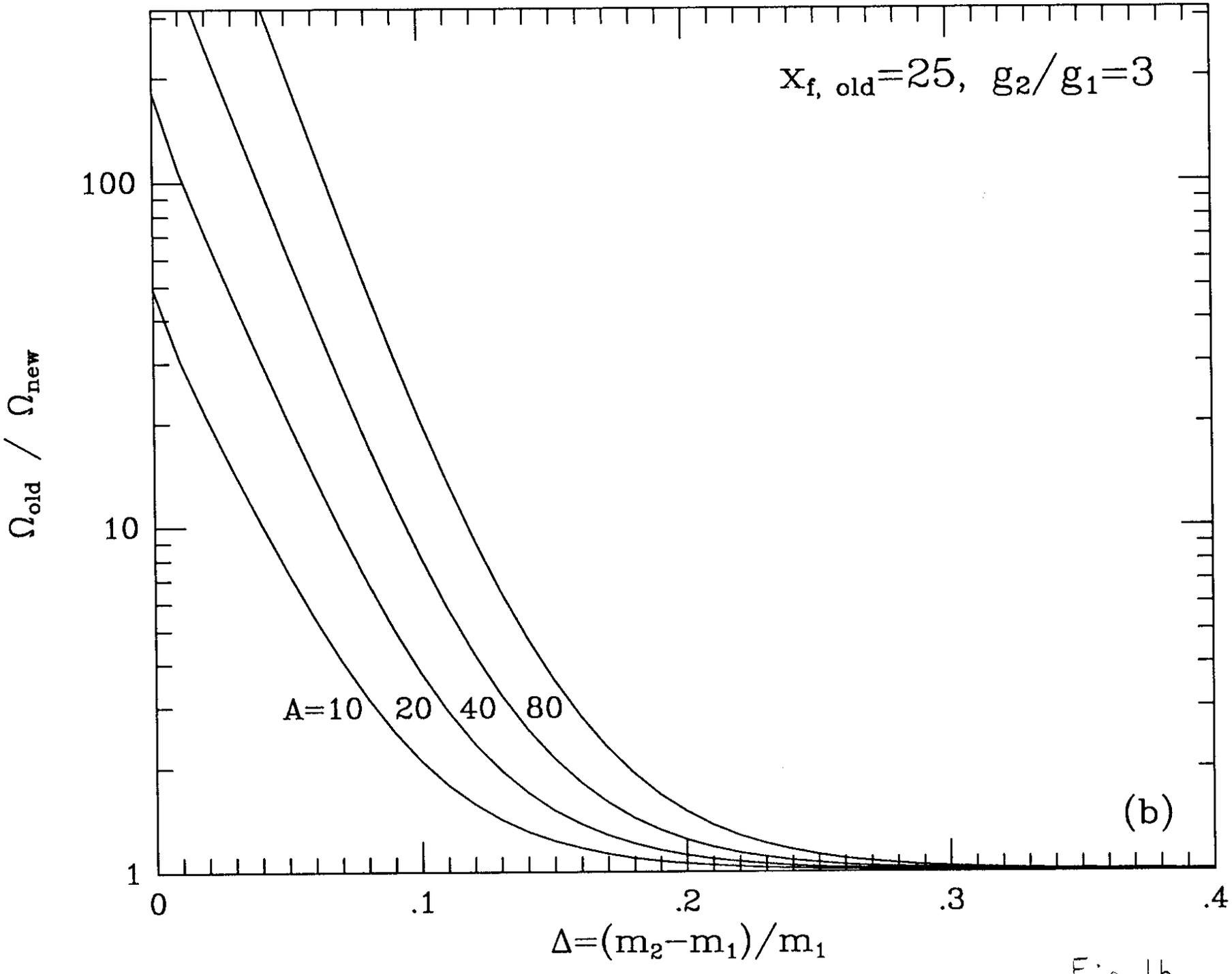
$x_{f,\ old}=25,\ g_2/g_1=3$
100
10
1
$\Omega_{old}\ /\ \Omega_{new}$
A=10 20 40 80
(b)
0
.1
.2
.3
.4
$\Delta=(m_2-m_1)/m_1$

Fig. 1b

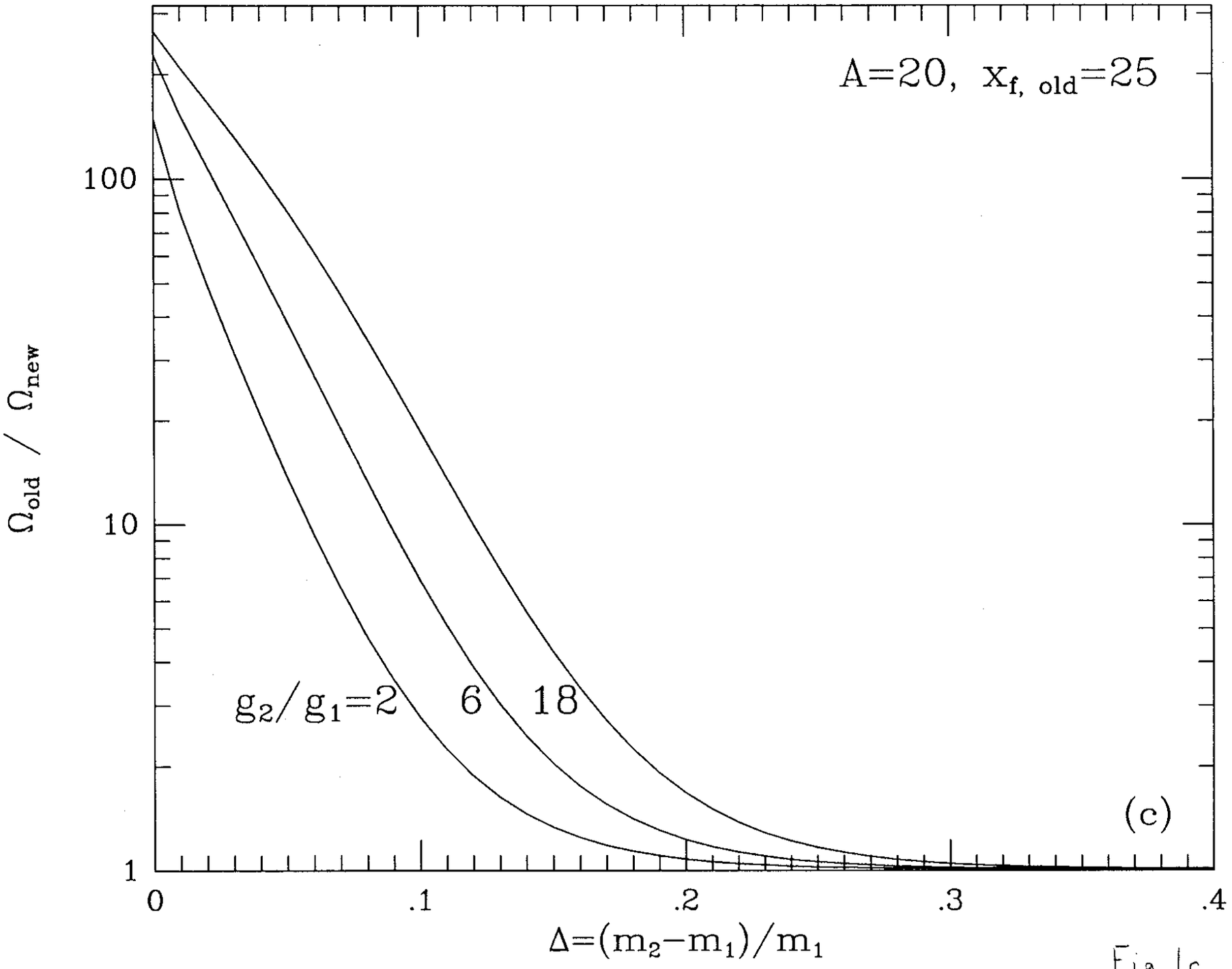
A=20, $x_{f,\ old}$=25
100
10
1
Ω_{old} / Ω_{new}
g_2/g_1=2
6
18
(c)
0
.1
.2
.3
.4
$\Delta=(m_2-m_1)/m_1$

Fig 1c

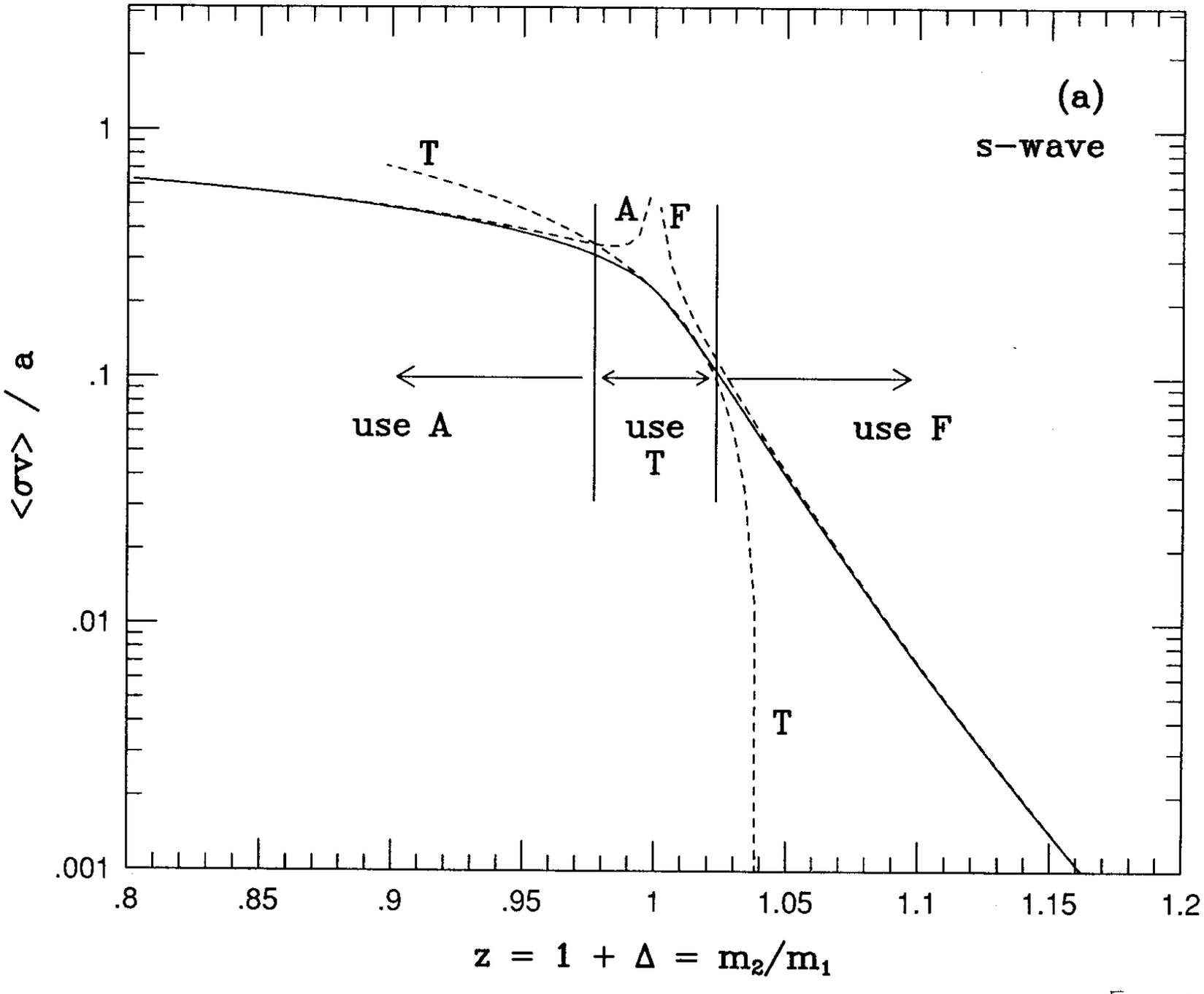
(a)
s-wave
T
A
F
T
use A
use T
use F
1
.1
.01
.001
.8
.85
.9
.95
1
1.05
1.1
1.15
1.2
<σv> / a
z = 1 + Δ = m2/m1

Fig. 2a

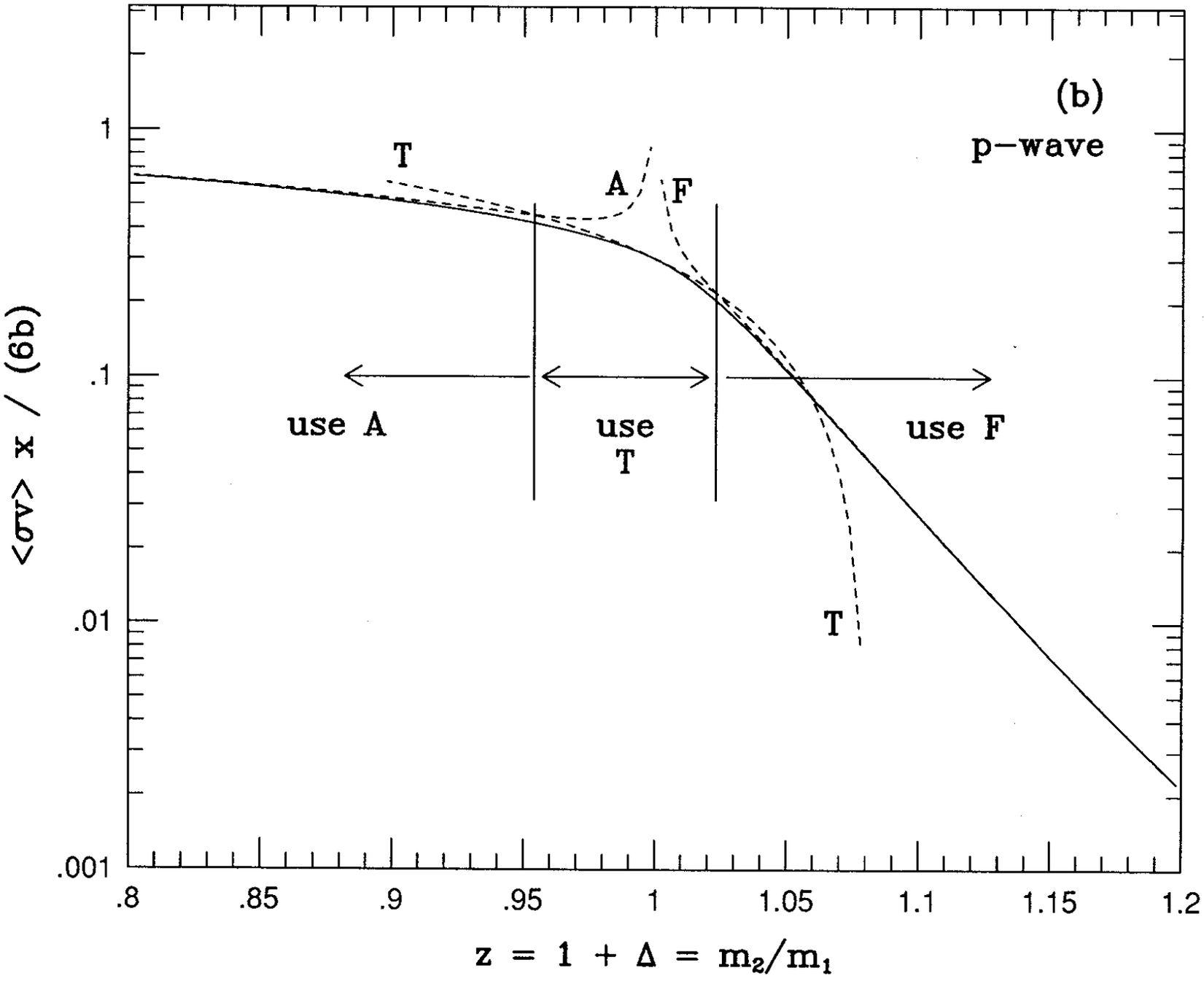
(b)
p-wave
T
A
F
T
use A
use T
use F
1
.1
.01
.001
.8
.85
.9
.95
1
1.05
1.1
1.15
1.2
<σv> x / (6b)
z = 1 + Δ = m2/m1

Fig. 2b

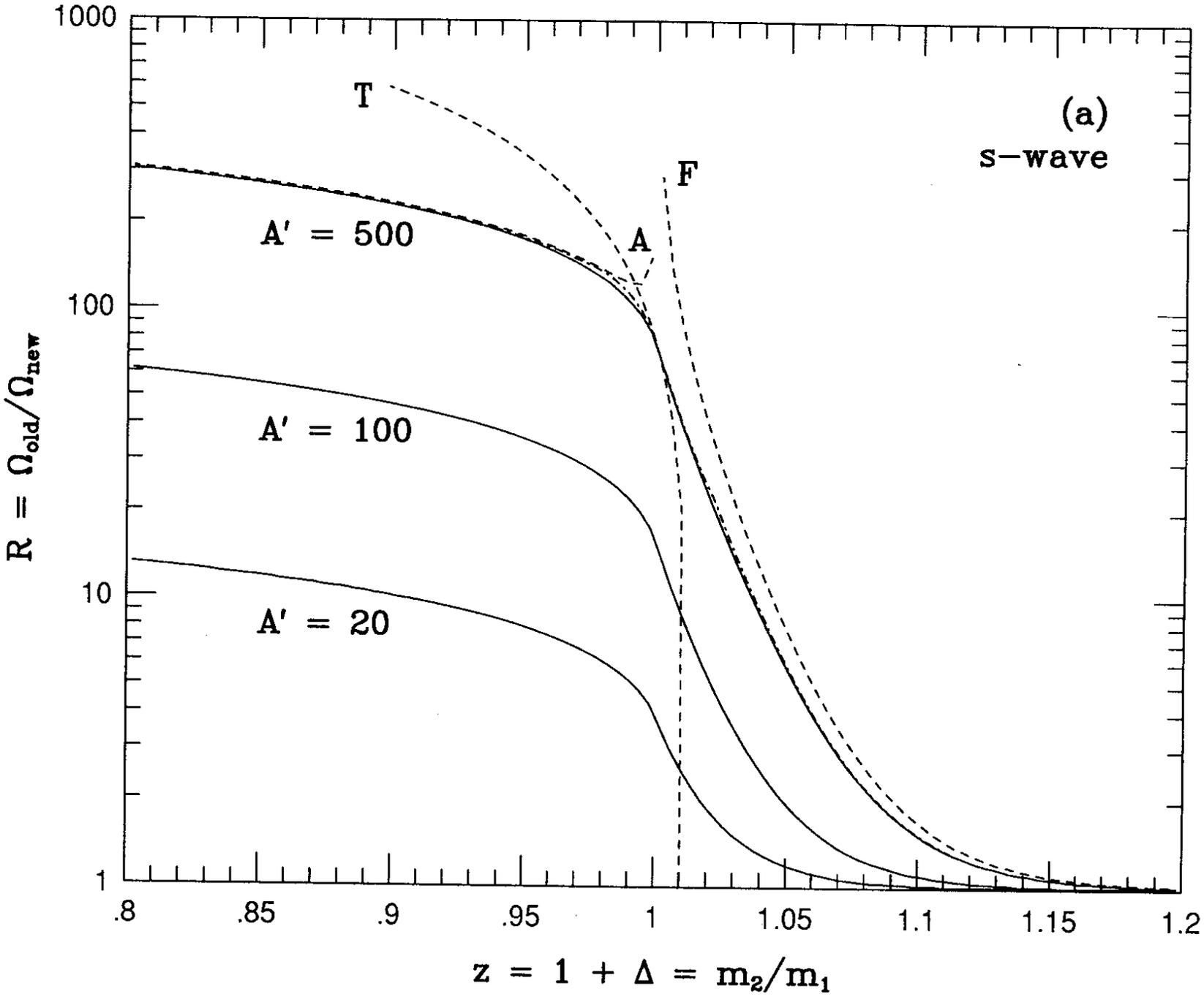
1000
100
10
1
T
F
A
(a)
s–wave
A′ = 500
A′ = 100
A′ = 20
R = Ω_old/Ω_new
.8
.85
.9
.95
1
1.05
1.1
1.15
1.2
z = 1 + Δ = m₂/m₁

Fig. 3a

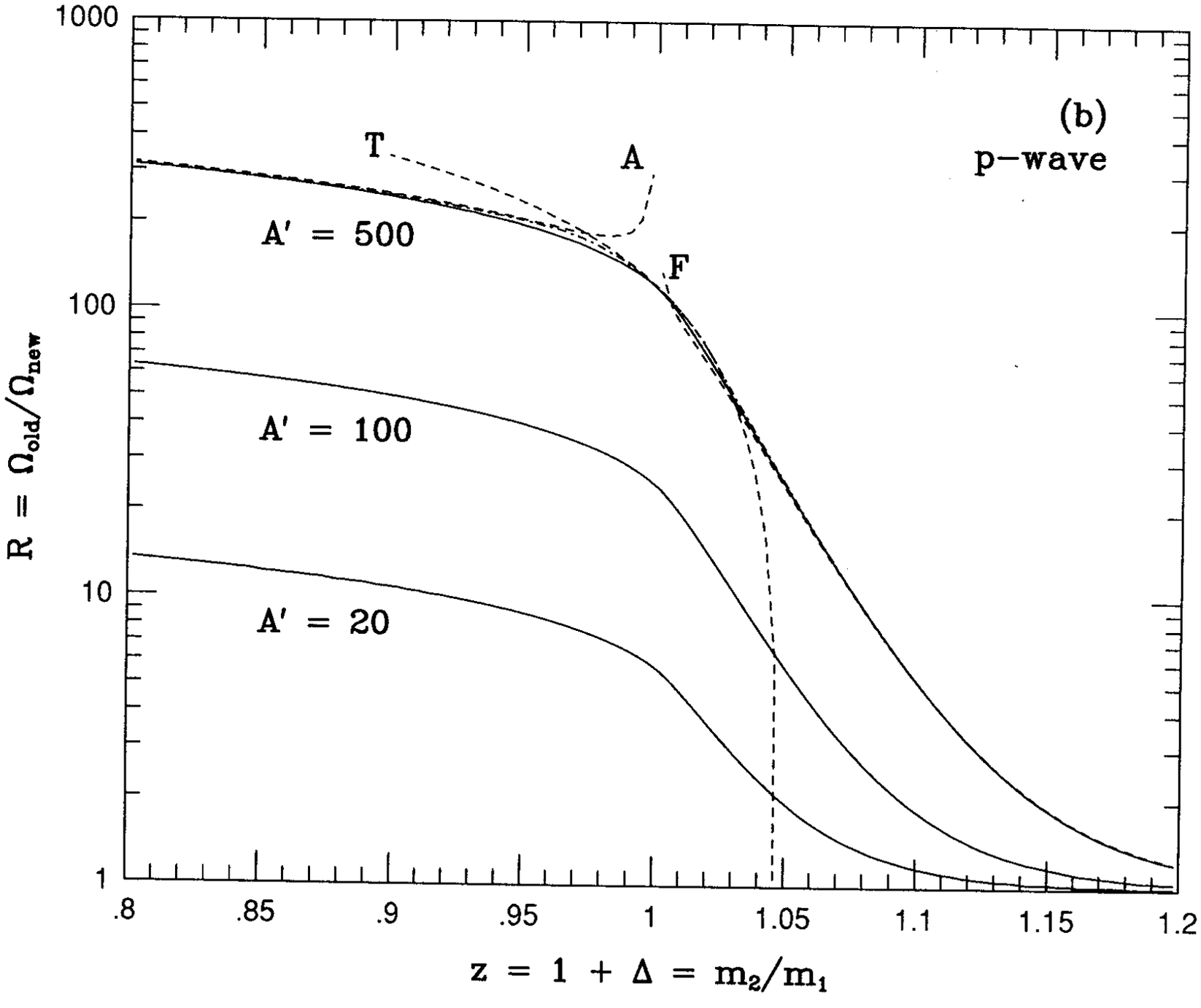
1000
100
10
1
(b)
p–wave
T
A
F
A′ = 500
A′ = 100
A′ = 20
R = Ω_old/Ω_new
.8
.85
.9
.95
1
1.05
1.1
1.15
1.2
z = 1 + Δ = m₂/m₁

Fig. 3b

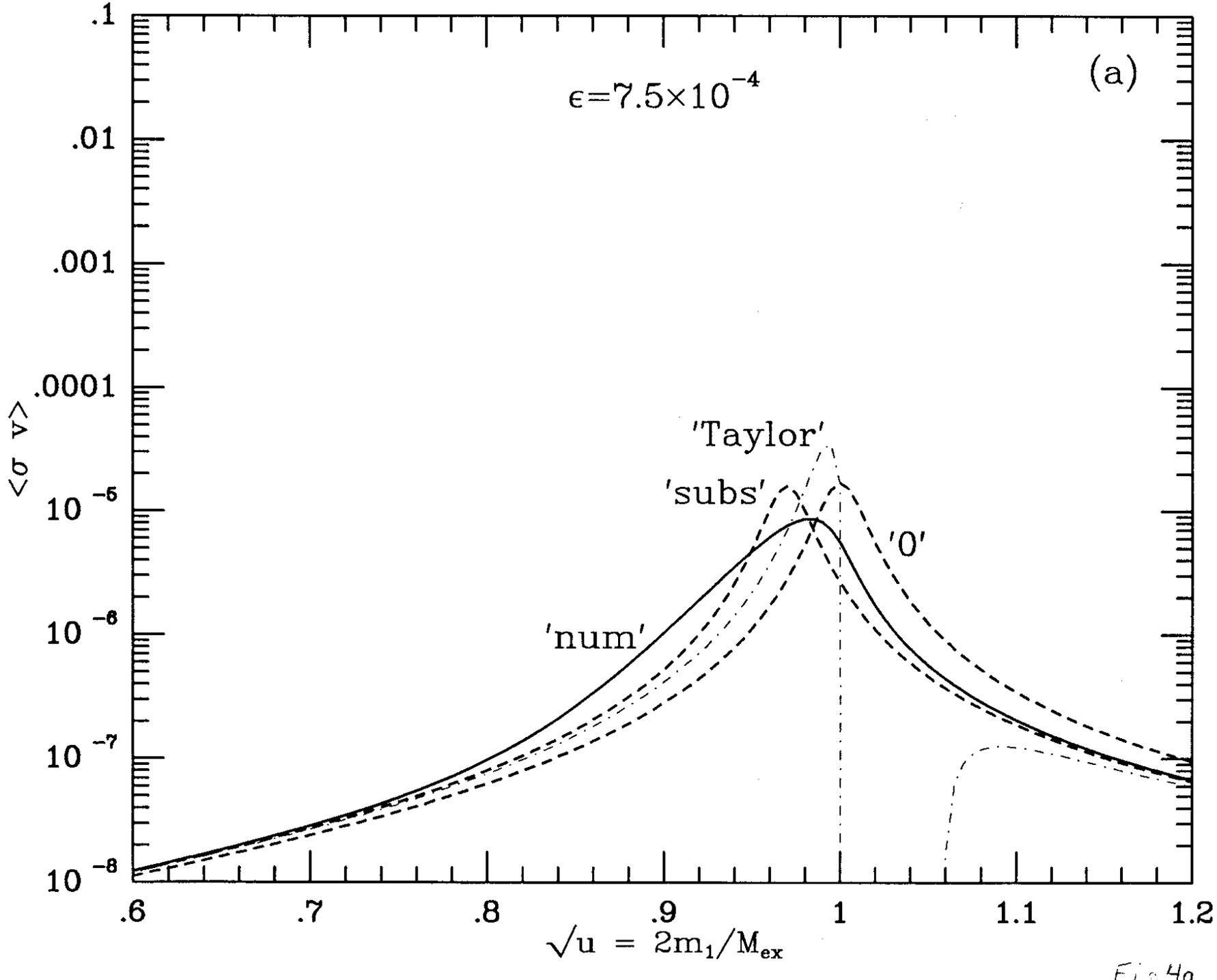
(a)
$\epsilon=7.5\times10^{-4}$
'Taylor'
'subs'
'0'
'num'
$\langle\sigma\ v\rangle$
.1
.01
.001
.0001
10^{-5}
10^{-6}
10^{-7}
10^{-8}
.6
.7
.8
.9
1
1.1
1.2
$\sqrt{u} = 2m_1/M_{ex}$

Fig 4a

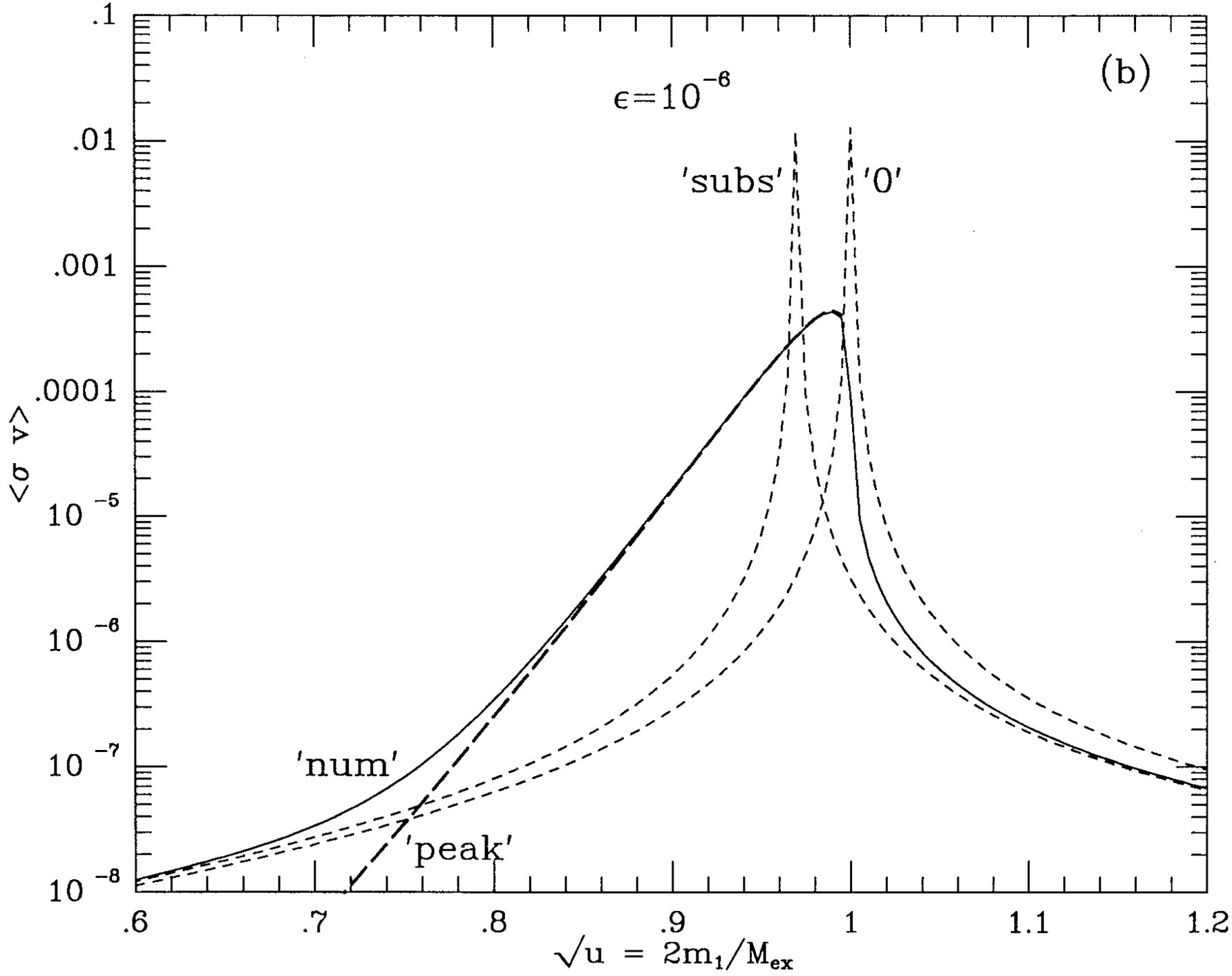
(b)
$\epsilon=10^{-6}$
'subs'
'0'
'num'
'peak'
$\langle\sigma\ v\rangle$
.1
.01
.001
.0001
10^{-5}
10^{-6}
10^{-7}
10^{-8}
.6
.7
.8
.9
1
1.1
1.2
$\sqrt{u} = 2m_1/M_{ex}$

Fig 4b

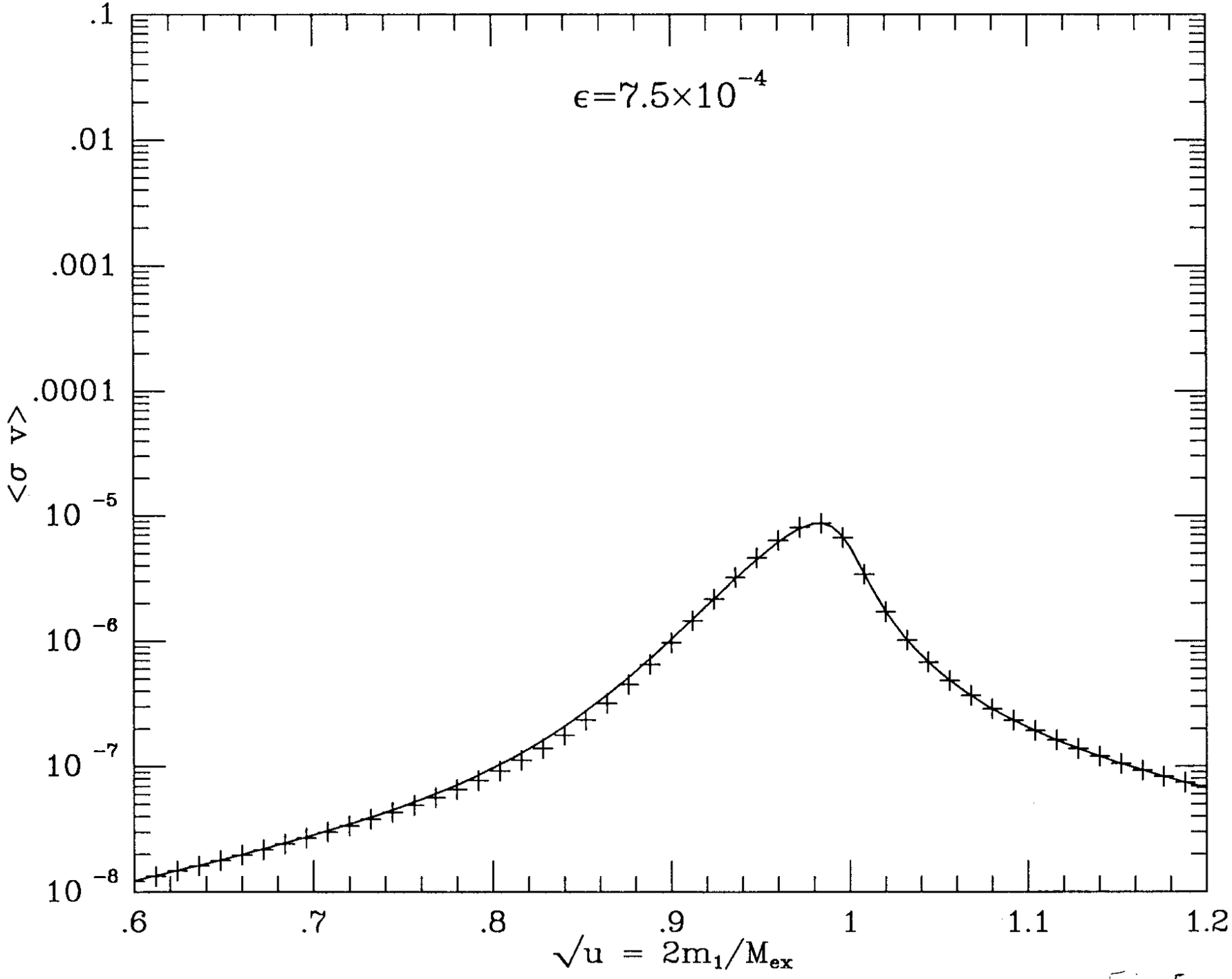
$\epsilon=7.5\times10^{-4}$
.1
.01
.001
.0001
10^{-5}
10^{-6}
10^{-7}
10^{-8}
$\langle\sigma\ v\rangle$
.6
.7
.8
.9
1
1.1
1.2
$\sqrt{u} = 2m_1/M_{ex}$

Fig 5

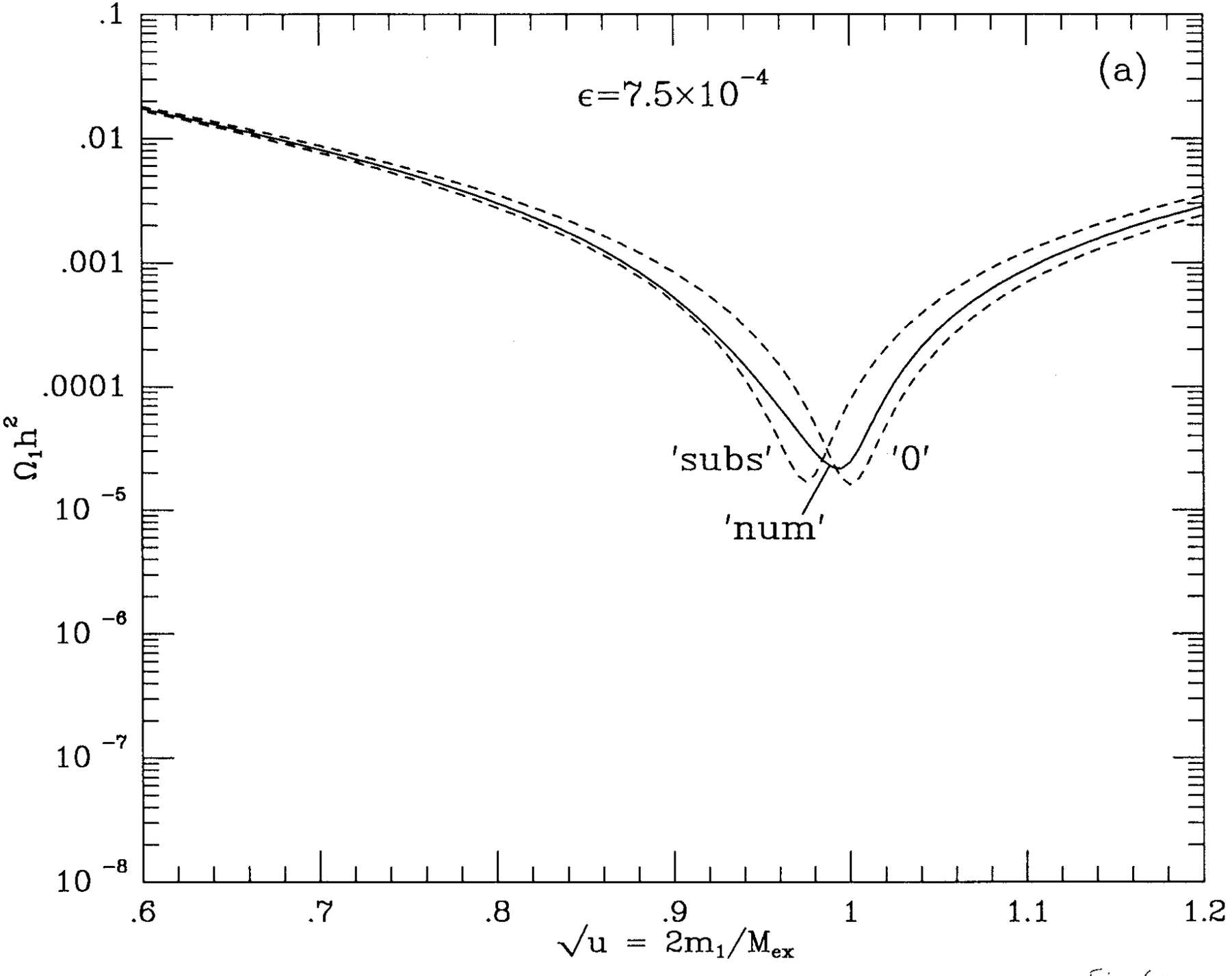
(a)
$\epsilon=7.5\times10^{-4}$
'subs'
'0'
'num'
$\Omega_1 h^2$
.1
.01
.001
.0001
10^{-5}
10^{-6}
10^{-7}
10^{-8}
.6
.7
.8
.9
1
1.1
1.2
$\sqrt{u} = 2m_1/M_{ex}$

Fig 69

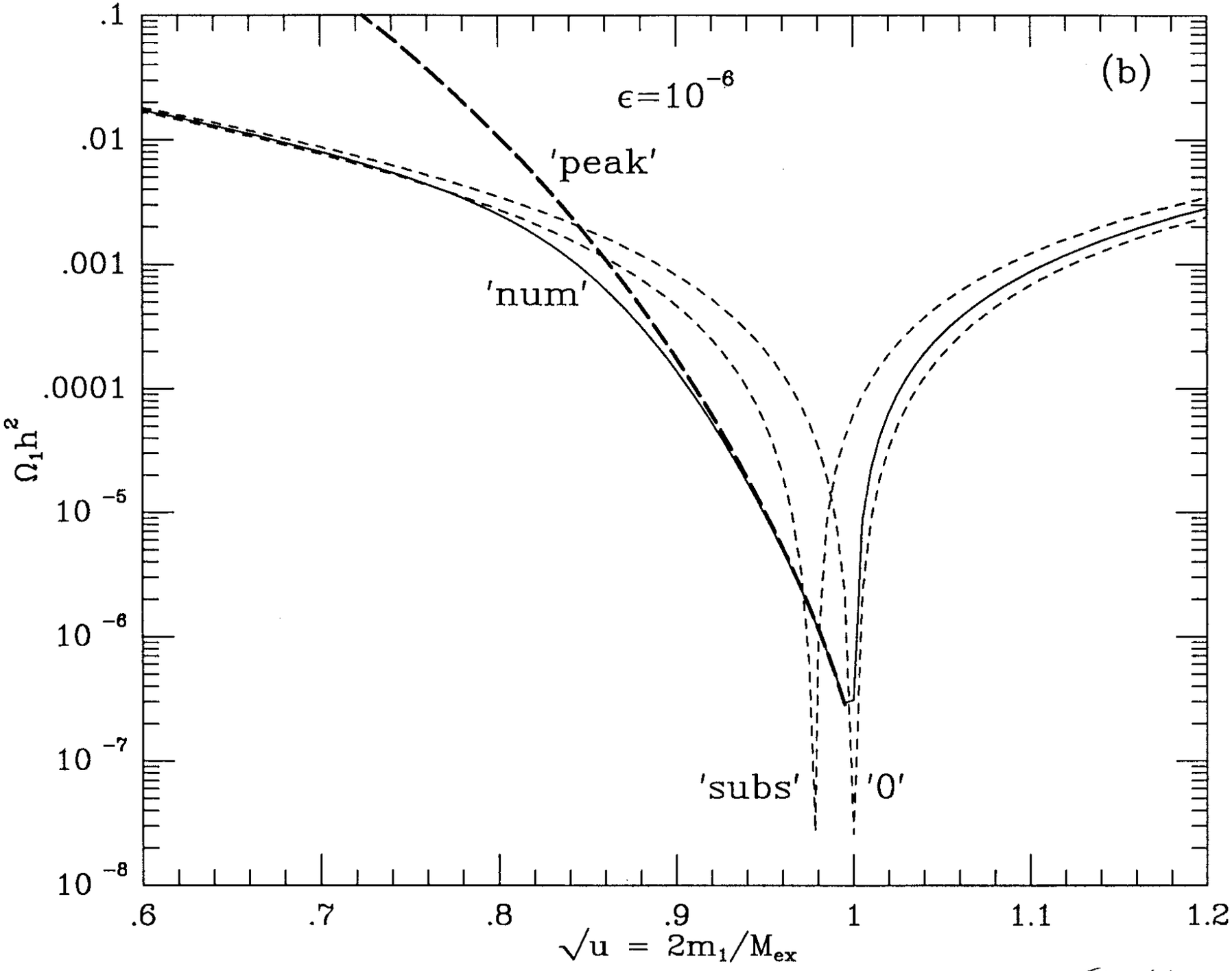
(b)
$\epsilon=10^{-6}$
'peak'
'num'
'subs'
'0'
$\Omega_1 h^2$
.1
.01
.001
.0001
10^{-5}
10^{-6}
10^{-7}
10^{-8}
.6
.7
.8
.9
1
1.1
1.2
$\sqrt{u} = 2m_1/M_{ex}$

Fig 66